ERDC/GSL TR-20-10

Geotechnical and Structures Laboratory

US Army Corps of Engineers®
Engineer Research and Development Center

ERDC
ENGINEER RESEARCH & DEVELOPMENT CENTER

*U.S. Air Force Rapid Airfield Damage Recovery (RADR) Program*

# Feasibility Investigation of Inductive Heating of Asphalt Repair Materials

Ben C. Cox, Web C. Floyd, John F. Rushing, Thomas A. Carr, and Craig A. Rutland

April 2020

**The U.S. Army Engineer Research and Development Center (ERDC)** solves the nation's toughest engineering and environmental challenges. ERDC develops innovative solutions in civil and military engineering, geospatial sciences, water resources, and environmental sciences for the Army, the Department of Defense, civilian agencies, and our nation's public good. Find out more at www.erdc.usace.army.mil.

To search for other technical reports published by ERDC, visit the ERDC online library at http://acwc.sdp.sirsi.net/client/default.

ERDC/GSL TR-20-10
April 2020

# Feasibility Investigation of Inductive Heating of Asphalt Repair Materials

Ben C. Cox, Web C. Floyd, John F. Rushing, and Thomas A. Carr

*Geotechnical and Structures Laboratory*
*U.S. Army Engineer Research and Development Center*
*3909 Halls Ferry Road*
*Vicksburg, MS 39180-6199*

Craig A. Rutland

*Civil Engineer Branch, Engineer Division*
*U.S. Air Force Civil Engineer Center*
*139 Barnes Avenue, Suite 1*
*Tyndall Air Force Base, FL 32403-5319*

Final report



Prepared for Headquarters, Air Force Civil Engineer Center
139 Barnes Ave., Suite 1
Tyndall AFB, FL 32403-5319

Under Project 463347, Rapid Airfield Damage Recovery (RADR) Program; MIPRs F4ATA76307GW01 and F4ATA76307GW01 AMD 1

# Abstract

Airfield pavement repairs conducted as part of rapid airfield damage recovery (RADR) activities must utilize suitable materials to reduce the need for subsequent repairs in order to maintain an operable pavement surface. For asphalt concrete pavements, hot mix asphalt (HMA) is typically used, but this requires a fairly large operation and is less practical for small repairs (e.g., small munitions damage, potholes). Instead, cold mix asphalt (CMA) is typically used for small repairs; however, its performance under aircraft loads is generally unacceptable.

The objective of this project was to investigate the feasibility of rapidly heating small-repair quantities (e.g., 5 gal buckets) of asphalt mix to hot mix temperatures in a matter of minutes. This objective was met using 15% steel aggregate by volume to produce an inductive HMA (iHMA) that could be heated from ambient to 320°F in approximately 5 min. This technology was demonstrated at full scale with a prototype field induction heater; iHMA patch repairs were subjected to simulated F-15E traffic and exhibited comparable rutting resistance to conventional HMA, which was considerably improved relative to CMA. Overall, iHMA was found to be a feasible repair material and should be considered for additional refinement and eventual implementation.

# Contents

# Figures and Tables

## Figures



## Tables

# Preface

This study was conducted for the U.S. Air Force Civil Engineer Center (AFCEC), Tyndall Air Force Base, FL, under Project Number 463347, Rapid Airfield Damage Recovery (RADR) Program; MIPRs F4ATA76307GW01 and F4ATA76307GW01 AMD 1. The program manager for this project was Dr. Robert Diltz of AFCEC. Mr. Jeb S. Tingle provided technical oversight of the project for ERDC.

The work was performed by the Airfields and Pavements Branch (GMA) of the Engineering Systems and Materials Division (GM), U.S. Army Engineer Research and Development Center, Geotechnical and Structures Laboratory (ERDC-GSL). At the time of publication, Dr. Timothy W. Rushing was Chief, GMA; Mr. Justin Strickler was Chief, GM; and Ms. Pamela G. Kinnebrew, GZT, was Technical Director for Military Engineering. Mr. Charles W. Ertle was Deputy Director, GSL, and Mr. Bartley P. Durst was Director.

COL Teresa A. Schlosser was the Commander of ERDC, and Dr. David W. Pittman was the Director.

The inductive hot mix asphalt (iHMA) technology developed under this study and described in this report has been filed with the U.S. Patent and Trademark Office under patent application number 15/265,507 titled, “Performance Grade Asphalt Repair Composition.” This patent application is pending as of the date of this report.

# 1 Introduction

## 1.1 Background

Rapid airfield damage recovery (RADR) includes recovery activities in response to an airbase attack to re-establish safe aircraft operations. Completing repairs in an expedient manner is key. Further, those repairs must utilize suitable materials, equipment, and construction techniques to reduce the need for subsequent repairs to maintain an operable pavement surface.

For asphalt concrete (AC) pavements, hot mix asphalt (HMA) is typically used for repairing bomb damage craters. In this case, crater upheaval is saw-cut and removed, rapid-setting flowable fill is wet-placed as a base layer, and then asphalt cookies are heated using a Bagela portable asphalt recycler to produce HMA. This HMA is placed into the crater repair and compacted using traditional methods and equipment such as double drum vibratory rollers. However, this process does not scale down efficiently and, for small repairs (e.g., small munitions damage or potholes), is much less practical (unless the equipment is already being utilized on the airfield for standard crater repairs as well).

For small AC repairs, materials and methods vary. For example, the standard tactics, techniques, and procedures (TTPs) for expeditious asphalt spall repairs outlined in the *Interim Process for Rapid Airfield Damage Repair, Revision 11.2* (USAF 2018) uses concrete spall repair materials and procedures, stating repairs are not likely to last 100 passes. In other cases, cold mix asphalt (CMA) is commonly used. For example, the U.S. Air Force (USAF) Sustainment Pavement Repair (SuPR) Kit contains over 40 5-gal buckets of Instant Road Repair, a CMA patching product. In a similar manner, CMA is probably the most common patching material for non-RADR repairs (e.g., for pothole repair on roads and highways).

Though HMA is the preferred material, CMA can be placed with relative ease and speed and is generally utilized when HMA is not available. Logistical advantages of CMA are generally outweighed, particularly for airfield repairs, by poor performance. CMAs require a curing period to develop stability but, even then, are still typically less durable and less rut resistant than HMA. From a highway industry perspective, CMA patches

are assumed to be temporary until semi-permanent repairs with HMA can be conducted. Past evaluations of commercial off-the-shelf (COTS) CMA products for airfield repairs have been less than favorable with CMAs withstanding fewer than 4 passes of F-15E simulated traffic 2 hr after patch placement (1 in. rutting failure criteria).

Because of the poor performance of CMAs, HMA is preferred when it is available. Challenges to obtaining small quantities (e.g., 5 gal bucket size) of HMA may include cold or rainy weather, lack of nearby asphalt plants, or the impracticality of firing up the full RADR asphalt operation for a small amount of HMA. A previous RADR research project identified pelletized asphalt, described in Saeed et al. (2009) and Cox and Sprouse (2019), as a potential solution for producing small quantities of HMA in the field. This technology has demonstrated the ability to be an effective solution and was fielded in the SuPR Kit. In an effort to further simplify the creation of small HMA batches at a significantly reduced time, this report presents another solution using inductive HMA (iHMA) that could be considered as a supplement to pelletized asphalt and, at the very least, a replacement to CMA.

## 1.2 Objectives and scope

The overall objective of this project was to investigate the feasibility of using induction heating technology as a mechanism to produce small quantities of HMA in a matter of minutes. The goal was to heat a 5 gal bucket of iHMA from ambient temperatures to 300°F (objective temperature – 250°F was threshold temperature) in approximately 5 min. Key tasks that were required in pursuit of this objective included the following:

1. Develop a portable induction heater unit that could be used in the field,
2. Identify a suitable container, or bucket, for iHMA that would not affect the inductive coupling between the heater and iHMA,
3. Identify and select suitable inductive materials to be included in the asphalt mix, allowing it to be heated inductively,
4. Design an appropriate asphalt mix that included inductive particles,
5. Perform full-scale field testing to evaluate all components simultaneously with particular focus on iHMA performance when subjected to simulated F-15E traffic.

This feasibility investigation included both laboratory-scale development and full-scale demonstration to show the concept is practice ready. The results of this study proved the feasibility of the overall concept; however, the concept was not fully evaluated in either area (laboratory or field). As a result, there is likely room for the iHMA concept to be further refined in later research efforts.

This project was conducted from January 2017 to January 2018 at ERDC, both in the asphalt materials laboratory and at the Outdoor Pavement Test Facility. Field evaluations occurred in January 2018.

## 1.3 Outline of chapters

Chapter 2 provides a literature review relating to patching procedures and materials as well as induction heating technology as related to asphalt. Chapter 3 describes the materials tested in this project, while Chapter 4 describes the experimental program. Chapters 5 and 6 present laboratory and field results, respectively. Chapter 7 provides a discussion of results, and Chapter 8 provides conclusions and recommendations.

# 2 Literature Review

## 2.1 Patching procedures and materials

### 2.1.1 State highways and municipal roads

From a state transportation agency and local municipality perspective, patching typically refers to pothole patching. According to Dailey et al. (2017), typical pothole dimensions are at least 1 in. deep with an equivalent diameter of 4 in. to 3 ft. This equates to a total volume of 1.4 gal on average up to 4.4 gal maximum.

Potholes are most problematic during winter months when pothole formation is accelerated due to freeze-thaw and adequate repairs are more difficult. During winter, agencies are generally limited to CMA patching materials, which could be either generic or proprietary, as HMA is not available in winter when asphalt plants are not in service (McDaniel et al. 2014, Dailey et al. 2017, Ghosh et al. 2018). The predominant mentality is that winter-season patches will be temporary because CMA is used, and the primary objective is simply to maintain safety and a reasonable ride quality even if only for a few months (i.e., until semi-permanent patches can be placed with HMA) (Dailey et al. 2017).

CMAs generally utilize cutback or emulsified asphalt binders that provide workability at ambient temperatures. However, workability comes at the cost of stability (rut resistance). The solvents or water used to provide workability also mean evaporative curing is required. In many cases, aggregate gradations are used which also promote workability during placement but are less stable under load. Distresses typically observed on patches include bleeding, dishing, debonding, raveling, and pushing or shoving due to lack of stability, with stability being identified as one of the most important characteristics of a good CMA (Prowell and Franklin 1995). Generally speaking, proprietary CMAs contain additional additives and outperform generic CMAs (Prowell and Franklin 1995), and, following conventional logic, HMA outperforms all CMAs (Dong et al. 2014, Ghosh et al. 2018).

Patch installation practices such as cleaning and drying a pothole, saw cutting to square up a pothole, and applying adequate compaction are important to achieve the best possible performance from the patching

material (Dailey et al. 2017). However, good practices are not always utilized (sometimes intentionally) in order to facilitate faster repairs and increase patching production rates.

There are four general types of patching repairs: throw-and-go, throw-and-roll, spray injection, and semi-permanent (Wilson and Romine 1999, McDaniel et al. 2014). The first two are generally considered temporary repairs with the third being somewhere in between temporary and semi-permanent. The throw-and-go method involves nothing more than shoveling repair materials into a pothole, and it is generally not recommended. The throw-and-roll method extends one step further by rolling over the patch with truck tires to provide some compaction. When considering all factors (i.e., not just repair performance but also repair time and productivity), throw-and-roll can be reasonably effective for higher-quality materials such as proprietary CMAs. Spray injection repairs utilize multi-process equipment to clean a pothole with air, tack with emulsion, and spray repair materials into a pothole.

The semi-permanent repair method is considered the best with respect to patching performance. This method generally suggests the use of HMA, meaning these repairs are not normally performed during winter (Dailey et al. 2017). This method also typically includes debris and water removal, saw cutting to square the pothole's edges, and a dedicated compaction method (i.e., a small roller or vibratory plate compactor rather than a truck tire).

With respect to repair timing, throw-and-roll repairs require, on average, 2.6 min per patch and yield a productivity of 1.6 tons per hour. In comparison, semi-permanent repairs require, on average, 13.3 min per patch and yield a productivity of 0.3 tons per hour (McDaniel et al. 2014). State agencies also reported in a survey in McDaniel et al. (2014) that times vary for planned and reactive patching activities. Most states reported 1 to 7 min for reactive patching (most likely more aligned with temporary patching) versus more than 30 min for planned patching (most likely more aligned with semi-permanent patching).

With regard to pothole patching, the phrase "do it right the first time" has been promoted among agencies as the best approach (McDaniel et al. 2014). This concept has been promoted because the cost effectiveness of a repair is significantly diminished when a patch must be replaced. Research and surveys of agencies have indicated investing in higher-quality repair

materials is economically advantageous if re-repairs can be minimized. The concept of using higher-quality materials up front is furthered by the fact that material costs are low relative to other patching-related costs (e.g., labor, equipment, and traffic control).

### 2.1.2 Airfields

Mejías-Santiago et al. (2010) tested seven COTS CMAs including Instant Road Repair (IRR) (supplied in the SuPR Kit), UPM Summer Grade, UPM Warm Summer Grade, Quality Pavement Repair (QPR®), EZ-Street® (EZ) EZ-Street® Hybrid, and Wespro. One objective was to develop laboratory certification tests and criteria to facilitate material acceptance in practice. Laboratory testing included flow time, flow number, tensile strength ratio (TSR), and workability testing.

The top four CMAs from laboratory testing (IRR, Wespro, EZ-Street®, and EZ-Street® Hybrid) were used to perform field patching. Patches were 3 ft by 5 ft and were 5 in. thick, placed in two lifts, each compacted with a vibratory plate compactor. Actual dimensions of each patch varied slightly, producing total repair volumes from 5.8 to 6.5 $ft^3$, or 43 to 49 gal, and requiring about 14 5-gal buckets of CMA each. Simulated F-15E traffic was applied 24 hr after patching; only one pattern of 16 passes was applied due to rut depths exceeding 1 in. and patch raveling. Ultimately, CMA was not recommended for airfield patch repairs subjected to heavy traffic or high tire pressure aircraft such as the F-15E.

Cox et al. (2017) evaluated nine COTS CMAs, seven of which were new relative to Mejías-Santiago et al. (2010). CMAs tested were IRR, EZ, AQUA PATCH (AP), Aquaphalt™ 6.0 (AQ), ChemCo Asphalt Repair (CCO), Instant Asphalt™ 6.0 (IA), Perma-Patch® (PP), QUIKRETE® High Performance Blacktop Repair (QR), and Ready Road Repair® (3R). Three of these (AP, AQ, and IA) were water-reactive proprietary formulations which typically contain plant-based oils and a reaction-assisting material. The manufacturer's directions call for water to be poured on the patches during installation, at which point the materials chemically react and promote strength development.

Laboratory wheel tracking with the Asphalt Pavement Analyzer (APA) was performed, a distinction from the tests considered in Mejías-Santiago et al. (2010). Water-reactive CMAs demonstrated notable rutting resistance relative to other CMAs, withstanding a full 8,000-cycle APA test compared

to less than 2,000 cycles. Among water-reactive CMAs, AP exhibited slightly higher rut resistance than AQ or IA.

IRR, AP, AQ, IA, and an HMA control mix were used for field patch repairs. Patches were 2 ft square and 4 in. thick, placed in two lifts and compacted with either a vibratory plate compactor or a single-drum roller. For simulated F-15E traffic applied 2 hr after placement, IRR rutted nearly 2 in. after 2 passes; AQ and IA exceeded 1 in. of rutting after 4 passes. For comparison, 4 passes on the HMA control yielded approximately 0.25 in. of rutting. In a later follow-up test of AP, AQ, and IA at 24 hr after patch placement, AP withstood 100 F-15E passes with just under 1 in. of rutting, while AQ and IA both exceeded 1 in. of rutting after 30 passes.

It was recommended to consider replacing IRR with a water-reactive CMA, preferably AP if possible as it withstood approximately three times more passes than AQ or IA. Shelf life was one concern for water-reactive CMAs but was not investigated in Cox et al. (2017). Little information is known regarding shelf life, but some indicators suggest shelf life of water-reactive formulations could pose challenges for long-term material storage. Ultimately, HMA was still recommended as the preferred patching material where possible.

## 2.2 Alternative asphalt heating methods

### 2.2.1 Microwave heating

Work done in Minnesota (Zanko et al. 2016, Latta 2013) evaluated microwave energy as an alternative heating method for increasing the temperature of asphalt patching materials. The inclusion of magnetite derived from taconite ore assisted the repair material in absorbing microwave energy and, consequently, increasing temperature. The system consisted of a 50 kW generator used to produce microwaves, a waveguide system to guide the microwaves to the repair location, and a steel shroud that contained the microwaves to the repair location. All components were mounted in the rear of a transport truck for field use.

First, the system was used to increase the temperature of the existing pavement, which eased debris removal and promoted bonding between the repair material and existing pavement. Next, asphalt repair material containing magnetite powder at 1.0 to 2.5% by mass was added to the repair location. Then, the truck-mounted microwave heater was operated

for several minutes atop the material. Once the repair material reached temperatures in the range of 250 to 300°F, the patching material was compacted and allowed to cool prior to opening it to traffic.

### 2.2.2 Induction heating

Rudolph et al. (2000) evaluated induction heating potential of carbon-fiber reinforced thermoplastics. Magnetic field intensity distribution was found to be the main influence on heating behavior and is highly related to power supply, coil geometry, and distance between the material and coil. Results indicated that a dispersion of conductive particles within a non-conductive medium (e.g., with respect to this project, asphalt) can be heated with induction energy.

Wu et al. (2005) evaluated the conductivity of HMA containing electrically conductive filler materials as a potential solution to thermoelectrically removing ice and snow from a pavement surface. Filler materials tested included carbon black, graphite, and carbon fiber with particle diameters of less than 150 microns. A series of HMA mixtures with conductive fillers were evaluated, and the most conductive mixture was determined to be some combination of filler and fiber. Note that this effort evaluated only conductivity, which relates to induction heating potential, but did not directly evaluate the potential for the mixtures to be inductively heated. Conductivity greatly and suddenly increased for most mixtures at approximately 5 to 12% by volume of asphalt binder. Though values were not provided, Wu et al. (2005) noted that there are practical upper limits to the filler contents that can be added without degrading an asphalt mixture's volumetric and mechanical properties.

Ahmedzade and Sengoz (2009) evaluated the mechanical and volume resistivity properties of steel slag coarse aggregate relative to limestone coarse aggregate for HMA. Results indicated that mechanical performance of steel slag mixtures was comparable to that of limestone mixtures, and that volume resistivity of the steel slag mixtures was lower than that of limestone mixtures, meaning steel slag mixtures may be suitable for applications in thermoelectrically and inductively heated asphalt pavements. However, it should be noted that ferrous content of industrial waste steel slag is typically low, and this may limit the material's potential for induction heating.

Garcia et al. (2009) examined the conductivity of asphalt mortar with conductive fillers and proved that these mixtures can be heated with induction energy. Asphalt mortars examined were composed of asphalt binder, sand, graphite, and/or steel wool. It was determined that steel wool fibers were more effective at increasing conductivity of the mixtures. Researchers demonstrated that 1.0 × 0.6 × 5.0 in. beams of sand asphalt and steel wool fibers could be heated inductively; mixtures containing 3.3, 6.1, and 8.8% steel wool fibers were heated to approximately 300, 420, and 465°F, respectively, in 3 min beneath a flat induction coil on a lab bench. Garcia et al. (2009) noted that the optimization of the inductive mixture would be dependent on the allowable heating time and desired temperature. While inductive heating rates were lower, it was not necessary for the mixtures to be electrically conductive to be compatible with inductive energy heating (which is an advantage over thermoelectrically heated pavements requiring conductivity for heat generation). It was noted that a potential application of this technology could be the increasing of the self-healing rates of asphalt pavements.

Liu et al. (2010) introduced type 1, type 00, and type 000 steel wool to porous asphalt mixtures for the purposes of heating the mixture using induction energy. Results of Cantabro mass loss testing indicated that the addition of steel wool fibers to the porous asphalt mixture increased particle loss resistance relative to the control mixture. However, the addition of steel wool fibers in sufficient volume to reach the maximum electrical conductivity for the different steel wool types effectively negates the particle loss resistance benefit provided by including the steel. A 50 kW induction heating system operating at 70 kHz frequency was used to evaluate induction heating potential of the porous asphalt mixtures. The coil utilized was flat, and surfaces of cylindrical test specimens were 1.25 in. from the coil. Specimens were heated for 3 min, and surface temperature was monitored with an infrared thermometer. Maximum surface temperatures reached at the end of heating cycles ranged from 279 to 405°F depending on the type and volume of steel fibers used. Further, it was proven that samples containing 10% type 000 steel wool by volume of bitumen could undergo healing from induction energy. These samples were cyclically loaded in indirect tensile fatigue tests until approximately 80% of the original stiffness remained. Following a 2 min induction energy heating cycle, it was reported that samples regained 100% of their original stiffness after cooling to the original test temperature.

Garcia et al. (2011) prepared asphalt mortar specimens with type 000 steel wool fibers. Gel-permeation chromatography indicated that changes in molecular weight of bitumen components following induction heating beneath a flat induction coil to 390°F were negligible. Although only limited data is presented, 1.0 × 0.6 × 5.0 in. asphalt mortar beams with 5.7% steel fibers by volume of bitumen regained more than 70% of their original stiffness through 6 cycles of induction energy healing after being fully broken in half. Garcia et al. (2011) recommended that volume fraction of fibers be determined experimentally for each mixture and suggested that the system may have applications for locations with very extreme winter weather conditions.

Liu et al. (2011) expanded on work done by Garcia et al. (2011) by evaluating induction healing potential of porous asphalt specimens that were not fully broken. Indirect tensile fatigue testing of mixes with 10% type 000 steel wool was performed at 40°F until the resilient modulus of the specimens was reduced by either 20 or 30%. The specimens were then exposed to induction energy beneath a flat induction coil for 2 min and rested for 24 hr. Then, specimens were tested in indirect tensile fatigue until the resilient modulus was reduced again by either 20 or 30%. The ratio of the number of cycles required after healing to the number of cycles required before healing to reach the same level of modulus degradation was termed the Healing Index. Liu et al. (2011) reported that the healing index of specimens with resilient modulus reduced by 20% or less could be 100%, meaning that all fatigue damage had been healed by induction energy.

Liu et al. (2012a) demonstrated the constructability of an induction healing porous asphalt mixture in a field setting by constructing a 1,300 ft test section. This section, located in the Netherlands, contained 1.3% type 00 steel wool by mass and was placed in December 2010. Laboratory characterization of the inductive mixture indicated that the addition of the steel fibers increased mixture durability, and no cracking was observed through the first two winter seasons in service (Liu et al. 2012b). Additional information related to the laboratory characterization of the material from the induction healing porous asphalt field mixture is available in Liu et al. (2013a).

Liu et al. (2013b) performed elastic foundation notched beam bending fracture testing on porous asphalt mixtures containing 4% type 00 steel wool by volume. After total fracture, specimens were heated with

induction energy beneath a flat coil to approximately 185°F over the course of 4 min to promote healing in the specimens. After healing, specimens were capable of recovering up to 78% of their original strength under the same test conditions as the original fracture.

Garcia et al. (2013) proved that dense graded asphalt concrete with steel wool could be heated using induction energy. Notched three point bending tests performed on 2.0 × 2.0 × 4.5 in. specimens were used to evaluate the healing level of specimens after initial testing to determine an appropriate healing temperature. Induction healing was accomplished by placing beam specimens beneath a flat induction coil. It was reported that the most appropriate method for healing was to raise and hold the temperature of the specimen above the Newtonian transition temperature of the bitumen. Garcia et al. (2013) noted that steel wool fibers increased thermal conductivity of the mixture to such a level that cooling levels may be too rapid and that inductive mixtures with lower thermal conductivity may be ideal for heat retention. It was also noted that steel fibers are difficult to mix, and future research may want to evaluate metallic aggregates.

The key finding from this literature review was that there are no previous studies where induction heating has been used in the manner it was used in this project. Many studies demonstrated that asphalt materials can be heated with induction technology when certain materials (e.g., steel wool fibers) are incorporated. However, these studies investigated inductively heated asphalt for different purposes (e.g., self-healing abilities) than in this project. As a result, different methods, such as flat induction coils, were used.

# 3 Materials Tested

## 3.1 Asphalt mixtures

Table 3.1 provides design properties of two conventional asphalt mixtures, termed AC1 and AC2. Both were typical Mississippi Department of Transportation (MDOT) mixes selected based on material availability.

Table 3.1. Hot mix asphalt concrete mix design properties.

| Mix Designation | | AC1 | AC2 |
|---|---|---|---|
| Purpose | | iHMA Reference Mix | Field Control Mix |
| NMAS | | 9.5 | 12.5 |
| $N_{des}$ | | 50 | 85 |
| PG Grade | | 67-22 | 67-22 |
| Percent Passing (%) | 1.0 in. / 25.0 mm | 100 | 100 |
| | 3/4 in. / 19.0 mm | 100 | 100 |
| | 1/2 in. / 12.5 mm | 100 | 97 |
| | 3.8 in. / 9.5 mm | 94 | 85 |
| | #4 / 4.75 mm | 61 | 56 |
| | #8 / 2.36 mm | 40 | 34 |
| | #16 / 1.18 mm | 29 | 26 |
| | #30 / 0.60 mm | 21 | 20 |
| | #50 / 0.30 mm | 10 | 13 |
| | #100 / 0.15 mm | 7 | 8 |
| | #200 / 0.075 mm | 4.9 | 5.4 |
| 3/4 in. Crushed Gravel (%) | | 0 | 5 |
| 1/2 in. Crushed Gravel (%) | | 62 | 70 |
| #11 Limestone (%) | | 7 | 0 |
| Coarse Sand (%) | | 10 | 8 |
| RAP (%) | | 20 | 11 |
| Hydrated Lime (%) | | 1 | 1 |
| Ag. Lime (%) | | 0 | 5 |
| $P_b$ (%) | | 5.9 | 5.2 |
| $P_{be}$ (%) | | 5.1 | 4.6 |
| $P_{ba,\ mix}$ (%) | | 0.8 | 0.6 |
| $V_{be}$ (%) | | 11.4 | 10.0 |
| $G_{mm}$ | | 2.385 | 2.376 |
| $G_{sb}$ | | 2.547 | 2.520 |
| $G_{se}$ | | 2.600 | 2.558 |
| $G_{sa}$ | | 2.646 | 2.636 |
| FAA | | 44.1 | -- |
| VMA (%) | | 15.4 | 14.0 |
| VFA (%) | | 74.0 | 71.4 |
| $P_{200}/P_{be}$ Ratio | | 0.97 | 1.18 |

*-- NMAS = nominal max. aggregate size*
*-- RAP = reclaimed asphalt pavement*
*-- $P_b$ = asphalt binder content*
*-- $P_{be}$ = effective asphalt binder content*
*-- $P_{ba,\ mix}$ = absorbed asphalt content*
*-- $G_{sa}$ = agg. apparent specific gravity*
*-- $G_{sb}$ = aggregate bulk specific gravity*
*-- $G_{se}$ = agg. eff. specific gravity*
*-- $G_{mm}$ = mix max. specific gravity*
*-- VMA = voids in mineral aggregate*
*-- VFA = voids filled with asphalt*
*-- $P_{200}/P_{be}$ Ratio = dust to $P_{be}$ ratio*

## 3.2 Mineral aggregates

Table 3.2 lists properties of AC1 mineral aggregates that were used in iHMA mixes. Because the Table 3.1 AC1 design was dated September 2014, aggregate specific gravities and absorptions were re-tested following ASTM C127 and C128 (2015) to obtain current values that were then used later during iHMA mix design trials.

Table 3.2. Properties of mineral aggregates used in AC1 mixture.

| Property | | 1/2" Crushed Gravel | #11 Limestone | Coarse Sand | RAP | Hydrated Lime |
|---|---|---|---|---|---|---|
| Percent Passing (%) | 1.0 in. / 25.0 mm | 100 | 100 | 100 | 100 | 100 |
| | 3/4 in. / 19.0 mm | 100 | 100 | 100 | 100 | 100 |
| | 1/2 in. / 12.5 mm | 100 | 100 | 100 | 99 | 100 |
| | 3.8 in. / 9.5 mm | 93 | 100 | 100 | 91 | 100 |
| | #4 / 4.75 mm | 53 | 93 | 98 | 68 | 100 |
| | #8 / 2.36 mm | 27 | 55 | 86 | 48 | 100 |
| | #16 / 1.18 mm | 15 | 41 | 76 | 40 | 100 |
| | #30 / 0.60 mm | 9 | 26 | 58 | 32 | 100 |
| | #50 / 0.30 mm | 6 | 18 | 15 | 15 | 100 |
| | #100 / 0.15 mm | 4 | 12 | 1 | 13 | 100 |
| | #200 / 0.075 mm | 2.8 | 11.1 | 0.5 | 6.9 | 100 |
| $G_{sb}$ | | 2.469 | 2.597 | 2.590 | 2.270 | 2.300 |
| $G_{sa}$ | | 2.639 | 2.718 | 2.644 | 2.355 | 2.300 |
| Abs (%) | | 2.59 | 1.66 | 0.41 | 1.59 | 0.00 |
| FAA | | 45.0 | 43.9 | 39.2 | 49.9 | — |

*-- Abs = water absorption (%)* *-- FAA = fine aggregate angularity (ASTM C1252 Method A [2017])*

## 3.3 Inductive steel aggregates

Multiple inductive materials were considered for their potential in an iHMA mix. In addition to providing the properties of the inductive materials ultimately selected for this project, this section summarizes other materials considered.

As discussed in literature review, previous inductive asphalt studies have primarily utilized materials consisting of small particles that act as fillers within the asphalt binder (e.g., steel wool fibers). However, the predominant goal of previous studies was to heat the asphalt binder component of the mix in order to heal any cracks that may have formed. Although these small particles may work well in a situation where heating the asphalt binder is the primary focus, they would likely not work well in a case where heating the entire mix for an extended period of time (i.e., long enough to place and compact) is of interest. The heat produced in the asphalt binder would dissipate quickly to the surrounding aggregates.

The predominant approach taken in this project was to replace a portion of the mineral aggregate with inductive "replacement" aggregates in order to provide greater thermal mass for heating the entire mix. During preliminary stages of this project, steel "coarse aggregates" were manufactured by cutting ½ in. and ¾ in. steel square bars into cubes with a band saw. These heated well inductively when dispersed in an asphalt mix; however, it was impractical to produce the range of particle sizes and overall quantities that would be needed for this project.

Slag aggregates, a waste byproduct from iron and steel processing, were considered as the particles resemble typical angular aggregate shapes. These have also been used elsewhere in asphalt paving as a type of recycled aggregate. Preliminary experimentation found the slag aggregates effectively did not heat inductively. On occasion, a slag particle might develop a small hot spot during heating, indicating a concentrated area of iron. Further investigation and discussions with suppliers indicated slag aggregate simply does not contain the iron content needed to be an effective inductive aggregate. By nature of the refining process, very little iron will ever be found in slag, and if it is, that slag will be recycled as the manufacturers do not want to waste iron.

Small, readily available steel particles appeared to be the most promising option as an inductive replacement aggregate. The shot blasting industry offers different variations of steel shot blasting and peening abrasives that can be purchased in bulk quantities and are available in a range of particle sizes, generally around that of a fine aggregate. These materials became the focus of this project. While coarse aggregates were also of interest, no commercially available materials in this size range were able to be identified.

Figure 3.1 provides photographs of four steel aggregates ultimately selected for this project. These represented different particle sizes and shapes and were ballast (B), cube shot (CS), cut wire (CW), and grit (G). Note that Figure 3.1 only shows the largest size fraction of each material so that particle shape characteristics are more apparent. Shot blasting abrasives are sold in a number of fairly narrow size ranges, meaning a size 120 grit, for example, contains essentially a single particle size. To create realistic fine aggregate gradations, multiple sizes were purchased of each steel type and were combined to form an overall well-graded material to the extent possible.

Figure 3.1. Photographs of steel aggregates tested.

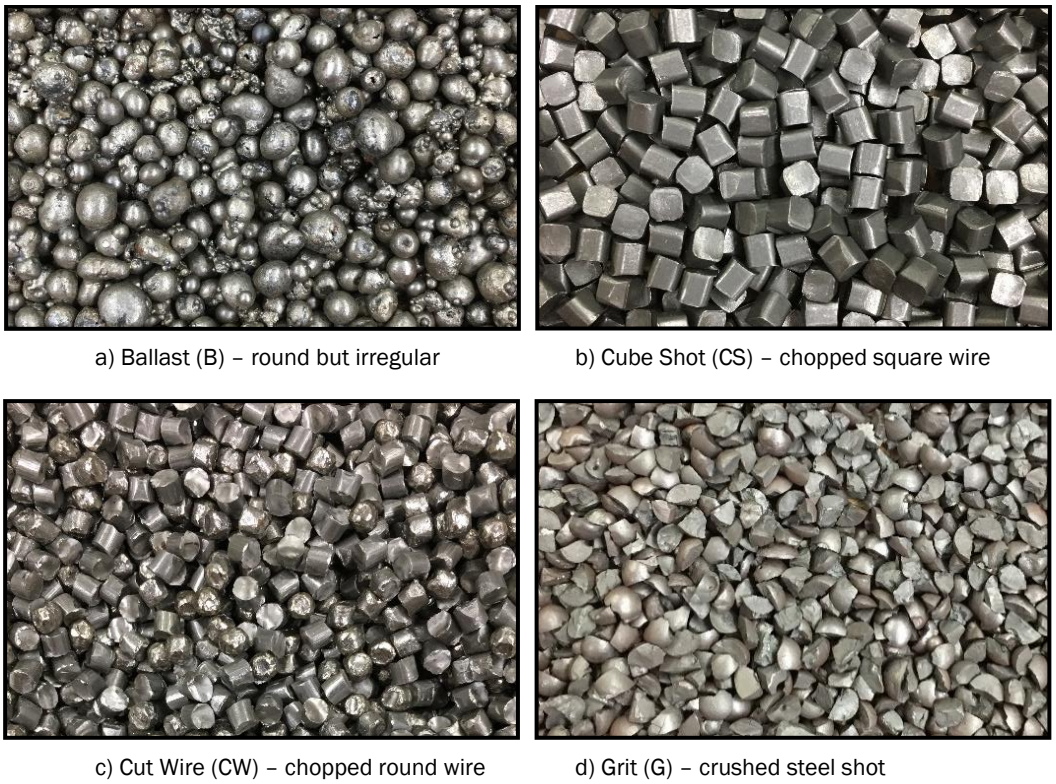

a) Ballast (B) – round but irregular

b) Cube Shot (CS) – chopped square wire

c) Cut Wire (CW) – chopped round wire

d) Grit (G) – crushed steel shot

Table 3.3 provides properties of the steel aggregates. When originally researching and purchasing steel materials, the plan was to consider, from a large order-of-magnitude perspective, the effect of particle size. As a result, steel aggregates were purchased in two size ranges that were 2.36 to 4.75 mm (#8 to #4) and finer than 2.36 mm (minus #8). B and CS were only available in a #8 to #4 size, whereas CW and G were available in both size ranges. For G, however, supplier data sheets were unclear, and what was thought to be in the #8 to #4 size range was actually mostly minus #8 (but larger than a #16). The decision was made to leave the test plan unchanged but rather to modify the terminology. Rather than referring to the larger class of steel as #8 to #4, this group was termed Size 1 steel, and the smaller minus #8 class of steel was termed Size 2 steel.

Table 3.3. Steel aggregate properties.

| Property | | Size 1 Steel | | | | Size 2 Steel | |
|---|---|---|---|---|---|---|---|
| | | B | CS | CW | G | CW | G |
| Individual Sizes Purchased | | S1320, S1110, S930 | BB, #2, #5 | 125 | G10 | 80, 47, 41, 32, 28, 20, 17, 12 | G12, G14, G18, G40, G80, G120 |
| Percent Passing (%) | 1.0 in. / 25.0 mm | 100 | 100 | 100 | 100 | 100 | 100 |
| | 3/4 in. / 19.0 mm | 100 | 100 | 100 | 100 | 100 | 100 |
| | 1/2 in. / 12.5 mm | 100 | 100 | 100 | 100 | 100 | 100 |
| | 3.8 in. / 9.5 mm | 100 | 100 | 100 | 100 | 100 | 100 |
| | #4 / 4.75 mm | 78 | 100 | 100 | 100 | 100 | 100 |
| | #8 / 2.36 mm | 3 | 0 | 0 | 90 | 100 | 100 |
| | #16 / 1.18 mm | 0 | 0 | 0 | 0 | 60 | 74 |
| | #30 / 0.60 mm | 0 | 0 | 0 | 0 | 30 | 43 |
| | #50 / 0.30 mm | 0 | 0 | 0 | 0 | 0 | 31 |
| | #100 / 0.15 mm | 0 | 0 | 0 | 0 | 0 | 9 |
| | #200 / 0.075 mm | 0 | 0 | 0 | 0 | 0 | 0.1 |
| $G_{sb}$ | | 6.558 | 7.839 | 7.753 | 7.390 | 7.753 | 7.390 |
| $G_{sa}$ | | 6.773 | 7.876 | 7.766 | 7.451 | 7.766 | 7.451 |
| Abs (%) | | 0.48 | 0.06 | 0.02 | 0.11 | 0.02 | 0.11 |
| FAA | | 36.5 | 38.1 | 37.8 | 47.1 | 37.8 | 47.1 |

Table 3.3 specific gravities ($G_{sb}$ and $G_{sa}$) were measured via ASTM C127 and C128 (2015) as would be performed for conventional aggregates, although this is undoubtedly extrapolating the test method beyond its intended use to some degree. Considering specific gravity of steel typically ranges from 7.75 to 8.05 g/cm$^3$ (though it can be lower depending on composition), CS and CW gravities appeared reasonable; however, values for B and G were suspect.

To rule out the influence of operator error, tests were repeated multiple times by different operators; however, between-operator differences were minimal and not meaningful. The difference between $G_{sb}$ and $G_{sa}$ represents the water absorption; if there is no absorption, then $G_{sb}$ equals $G_{sa}$. Since absorption for steel should be essentially negligible, $G_{sb}$ and $G_{sa}$ should be able to be used interchangeably in theory. Even still, $G_{sa}$ for G was lower than expected for typical steel. For B, its absorption value was at least plausible based on its surface texture, which contained numerous void-like imperfections that tended to trap water (i.e., these imperfections acted like pores). Ultimately, a good faith effort was made to address the unusual results and uncover any potential testing issues, but none were found. Because the actual composition of these materials is unknown, the measured Table 3.3 gravities were taken as representative and were used throughout the project.

Table 3.3 FAA values were determined by ASTM C1252 Method A (2017) except for B and CS. These two required Method C, which is used for #8 to #4 particle sizes. Based on visual observation, it was expected that CS and G would exhibit the highest angularity, B would exhibit the lowest, and CW would be somewhere in the middle. This trend was true for all but CS; however, FAA values for CS are believed to be incorrect. Due to its larger cubical shape, CS would not flow freely through the C1252 funnel as the test intended. Particles would interlock and not flow unless agitated. Therefore, a spatula had to be used to gently stir the funnel contents. The test does not allow for this type of action because any vibrations to the overall test setup would encourage consolidation of CS collected inside the brass measure. While care was taken to avoid consolidation, it was inevitable and is expected to have produced a lower FAA as a result.

Overall, several challenges to traditional aggregate testing were encountered during steel aggregate testing. $G_{sb}$, in particular, is a very important volumetric property as it has great implications with respect to asphalt binder demand. These challenges are perhaps areas that should be investigated further in later studies.

# 4 Experimental Program

## 4.1 Equipment and supplies

### 4.1.1 Induction heaters

Two induction heater systems were used in this project: a laboratory induction heater (LIH) and a field induction heater (FIH). The LIH system (Figure 4.1) utilized a 15 kW Ambrell EKOHEAT® 15/100C power supply (480 V, 3 ph) that was used in conjunction with a four-turn copper induction coil designed by Ambrell Corporation for this project. The EKOHeat® 15/100C power supply possesses an auto-tuning frequency range of 50 to 150 kHz. Multiple settings can be adjusted on the power supply to influence the rate at which the material in the coil heats; key parameters are the input voltage and the RF tap selection. These parameters in particular affect the resulting output power and, to some degree, the coupling match between the electromagnetic field and material (other factors such as air gap also affect coupling match).

Figure 4.1. Laboratory induction heater (LIH) system.


a) EKOHEAT(R) 15/100C power supply b) Laboratory induction coil

Figure 4.2 provides an overview of the FIH system that was designed and built by Ambrell Corporation with ERDC input and guidance for this project. The same 15 kW EKOHEAT® power supply was used but with a larger workhead capacitor (the workhead is the black box protruding from the red induction coil enclosure in Figure 4.2a). The FIH coil was completely enclosed for safety purposes, and its inside was sleeved to prevent snags when loading iHMA containers. The induction heater requires circulating water to cool its internal components during

operation. For the LIH, continuous-flow tap water could be used; for the FIH, it requires an onboard water-cooled heat exchanger (Figure 4.2a), which was a Dimplex Thermal Solutions SVI-5000-M (460 V, 3 ph).

Figure 4.2. Field induction heater (FIH) system.

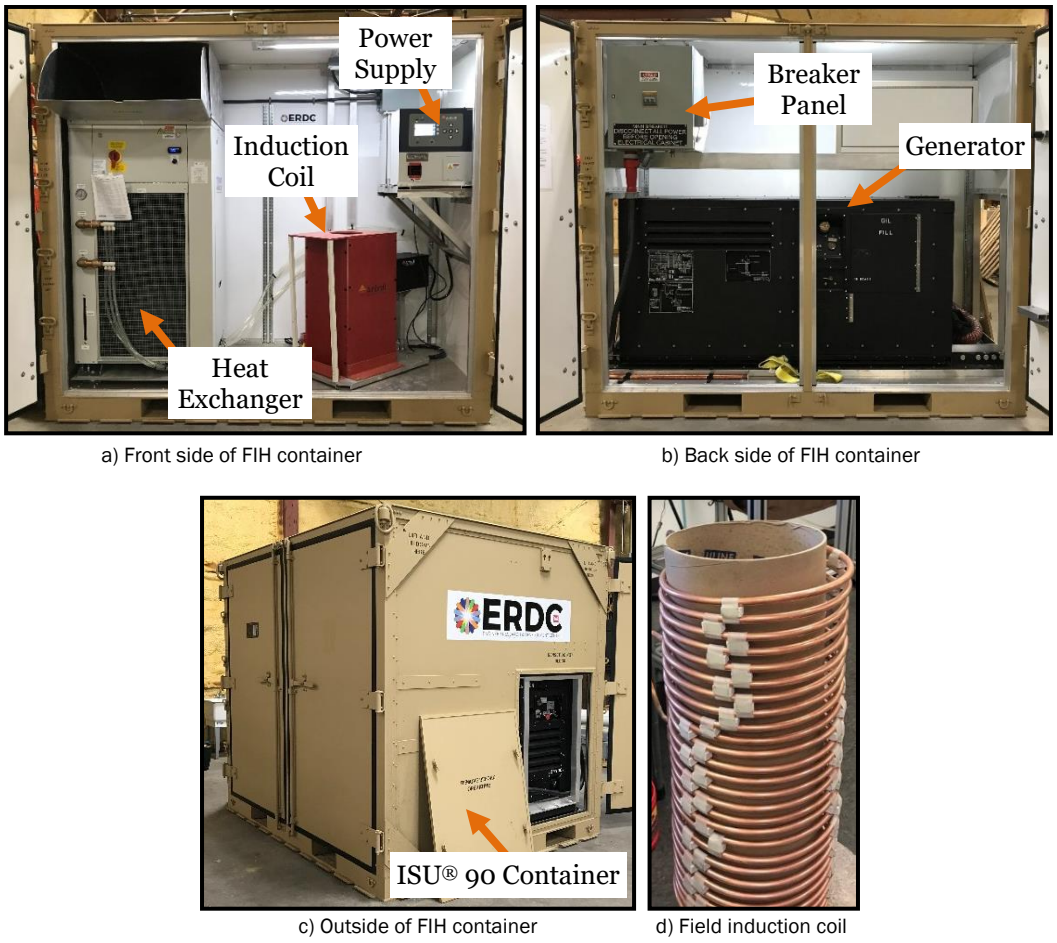


a) Front side of FIH container

b) Back side of FIH container

c) Outside of FIH container

d) Field induction coil

Figure 4.2b shows the back side of the FIH, which houses a 35 kW diesel generator producing 480 V of 3 phase power and a breaker panel. The entire FIH system is contained inside an ISU® 90 container that can be top-lifted, forklifted, or locked into cargo rail systems on aircraft such as the C-17A Globemaster III. Figure 4.2d shows the copper induction coil designed by Ambrell for a 5 gal container with the coil enclosure and sleeve insert removed.

### 4.1.2 Mix containers

Selection of a container for iHMA was a key task in this project. Proprietary CMAs like Instant Road Repair in the SuPR kit or AQUA PATCH recommended in Cox et al. (2017) utilize conventional HDPE plastic buckets,

which would melt at hot mix temperatures. Metal buckets are typically used for HMA; however, early discussions with Ambrell Corporation indicated these would interfere with the coupling of the induction heater to the iHMA. A container that would neither melt nor interfere with induction heating needed to be identified. Further, it was a goal of this project to first investigate container options that were already commercially available as anything that was not could likely be cost prohibitive.

A market survey was conducted to identify other types of containers that might be suitable. In the very preliminary stages of this project, large glass beakers (e.g., 10 L or 2.6 gal) were used; of course, these are not durable and would not be a good long-term solution. Other materials were considered such as high-temperature plastics; however, no COTS containers were identified. Ultimately, fiber containers such as fiber drums, mailing tubes, or Sonotubes® were selected. Figure 4.3 shows three different sizes used in this project. Fiber containers do not melt or interfere with the induction heating, they are readily available in a variety of sizes, and they are fairly economical. Costs are on the order of typical HDPE plastic buckets, meaning the containers are cheap enough for one-time use (i.e., disposable).

Figure 4.3. Fiber containers for iHMA.

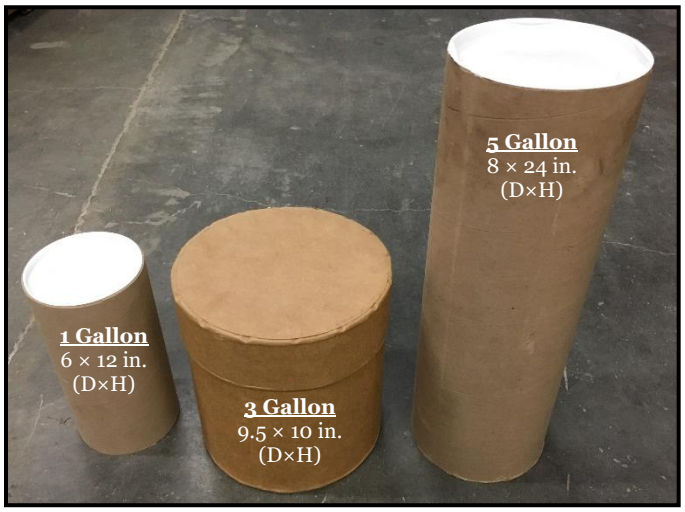


The 3 gal drum shown in Figure 4.3 was originally purchased to fit snugly in the LIH coil as shown in Figure 4.4. It consists of fiber walls and bottom and a fiber lid. Its size, yielding only a small air gap between the container and coil, would maximize heating efficiency. Similar containers in a 5-gal size were also evaluated for the FIH use but were ultimately not used.

Figure 4.4. A 3 gal fiber drum inside the LIH coil.

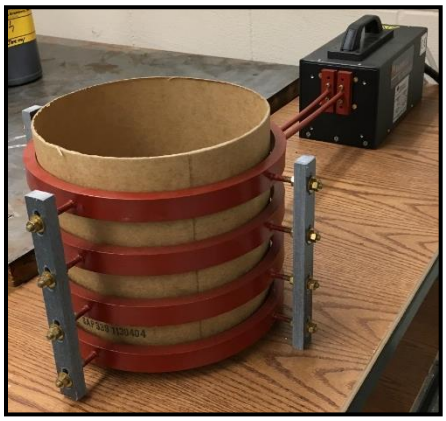

During the laboratory phase of this project, it was discovered that reasonable induction heating could be achieved in the 1 gal tubes shown in Figure 4.3, even though a much larger air gap was created (Figure 4.1b). Use of the smaller 1 gal containers provided considerable material quantity savings and facilitated more efficient testing. Whether 1 or 3 gal containers were used, inevitably the results would not directly scale up to a 5-gal FIH size container; therefore, laboratory container size was less critical so long as results were reasonable. Ultimately, 1 gal containers were used for most laboratory testing.

Fiber tube cotainers, whether 1 or 5 gal, were essentially large mailing tubes with a 1/8 in. wall thickness. Either 6 or 8 in. diameter tubes were purchased and cut to either 12 or 24 in. lengths, respectively. Plastic end caps were supplied with the mailing tubes (shown in Figure 4.3). While these could be used as caps or lids for the top of each tube, they were inadequate for the bottom. Instead, other available tube plug options were reviewed, and wooden plugs were selected. Figure 4.5 shows fiber tube specifics including details of the wooden plugs. Plugs were 6 1/16 or 8 1/16 in. diameter cut from ¾ in. plywood. A 7° taper was cut around the circumference to the mid-depth of the plug to facilitate insertion into the tube end. Plugs were tapped into place using a hammer or mallet. Plug retention was found to be more than sufficient to hold, in the case of the 5 gal tube, 5 gal of iHMA materials. While similar plugs can be purchased commercially, the plugs used in this project were cut as needed by ERDC's model shop.

Figure 4.5. Fiber tube container details.

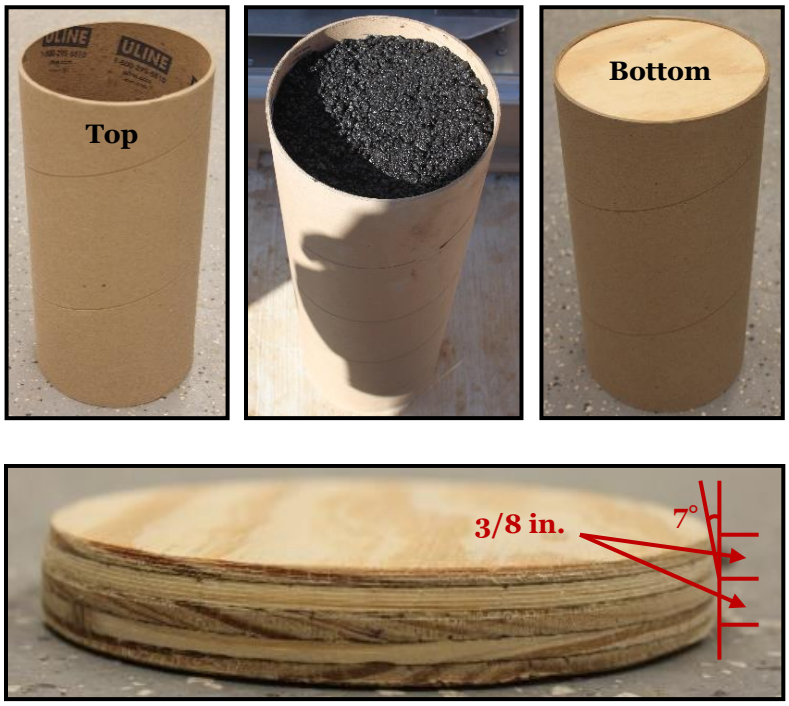


### 4.1.3 Compaction equipment

Two pieces of compaction equipment (Figure 4.6) were used in this project. A Pine Instruments AFGC125X gyratory compactor was used for laboratory compaction, and a Northern Industrial JPC-80 vibratory plate compactor was used for field patch compaction.

Figure 4.6. Compaction equipment.

a) Laboratory compaction b) Field compaction

## 4.2 Test methods

### 4.2.1 Convection and induction heating methods

Standard laboratory convection ovens as shown in Figure 4.7 were used for various portions of the project. All laboratory-compacted iHMA (i.e., materials used during mix design) was oven heated to 320°F prior to mixing in a 5 gal bucket mixer and compacting at 300°F. Field-compacted iHMA was laboratory-produced, meaning it was oven-heated to 320°F, mixed in a 5 gal bucket mixer, and then placed in 5 gal fiber tubes where it was allowed to cool and stored until the field evaluation. Other HMA materials such as that used for field testing were oven-heated as well.

Figure 4.7. Laboratory oven.

For induction heating, the machine settings (i.e., input voltage and RF tap) were first established. These settings are specific to the power supply, workhead, coil, and material used; however, once they are established, they should hold true for any system. For example, the common user does not have to adjust machine settings; they would be set for the given heater system and material beforehand. Another setting that can also be controlled is the run time, which can be set on a countdown timer. Again, this could be set in advance for the common user.

Multiple machine setting combinations were investigated in the early stages of this project. For the LIH, an input voltage for 928 V was ultimately used with an RF tap selection of 18. In Experiment 2 described in Section 4.3.1, these settings resulted in a power response of 3.3 to 5.8 kW (4.6 kW average) depending on the coupling match, which ranged from 41 to 59% and averaged 50%. These modest matches were due to the increased air gap when using a 1 gal container in a coil designed for a 3 gal

container (Figure 4.1b). For the FIH, an input voltage of 1,100 V was ultimately used with an RF tap selection of 10. This provided a typical power output of 14.1 kW, which was just under the total 15 kW capacity of the machine, and a 100% coupling match.

Once machine settings were established, the induction heating method was fairly simple. For the LIH, water flow to the system was turned on, the EKOHEAT® was turned on, the sample container was set inside the coil (centered), and then the start button on the machine's front panel was pressed.

For the FIH, the generator was first cranked and given several minutes to warm up, then the heat exchanger was turned on, followed by the EKOHEAT®. The sample container was then lowered into the coil as shown in Figure 4.8 before pressing start on the front panel.

For this project, 1 in. nylon flat webbing was used to create a sling for inserting or removing the iHMA container from the FIH coil. There was just enough gap between the coil and container to do so, and the insulating properties of the container prevented the webbing from becoming too hot.

Figure 4.8. Placing 5 gal iHMA tube into FIH coil.

Other loading/unloading concepts were discussed. Manual lifting could be eliminated by using a small hoist mounted along the ceiling of the container. A 500 lb capacity wire rope hoist with a lifting speed of 15 fpm was installed, but manual lifting was actually preferred during field testing because it was faster.

Another concept was to install the coil assembly on a vertical roller track with some sort of counterbalance or assisted lift device. This would allow the entire coil assembly to be lifted up to the top of the container with little effort. An iHMA container would be set on the container floor in the correct position, and then the coil would be lowered down around the container for heating. This concept was devised after the FIH coil assembly was already designed, and there were insufficient funds for the work needed to implement this concept. It was, however, agreed upon by both ERDC and Ambrell that using a moveable coil should be considered in future iterations of the FIH.

### 4.2.2 Thermal measurements

Thermal measurements were obtained in one of two manners. First, infrared measurements from a FLIR E8 hand-held camera (Figure 4.9) were used to measure surface temperatures. Second, thermocouples were used to measure internal temperatures using the setup shown in Figure 4.10.

Figure 4.9. FLIR E8 infrared camera.


In the case of Figure 4.10a, four thermocouples (TCs) were affixed to a ¼ in. wooden dowel at various depths of 1, 4, 6, and 8 in. from the bottom of the 1 gal container. TCs were epoxied onto the dowel with their tips bent slightly outward to ensure good contact with the surrounding mix. Without covering TC tips, the dowels were wrapped with electrical tape or duct tape to further secure the TCs. TCs were plugged into a Campbell Scientific data acquisition system (Figure 4.10b), and data was recorded at a sampling rate of 1 Hz.

Figure 4.10. Thermocouple temperature measurement setup.

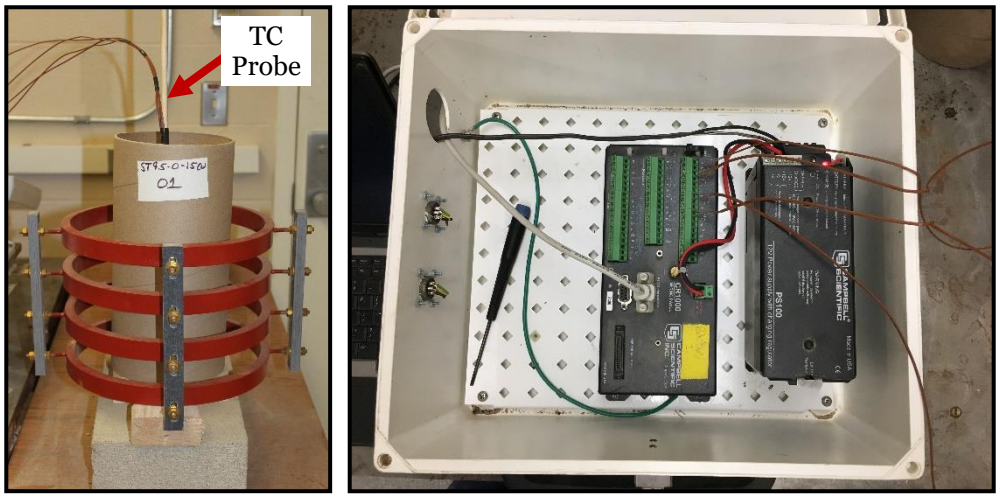


a) Thermocouple probe in mix b) Data acquisition system

### 4.2.3 Laboratory mix design processes

Volumetric mix design was performed following standard Superpave procedures. Mixing temperature was 320°F, compaction temperature was 300°F, and the design air void ($V_a$) level was 4% at a design gyration level ($N_{des}$) of 50 gyrations, following the same design parameters as AC1 (Table 3.1). The primary difference between AC1 and iHMA designs was that steel aggregates were included in addition to the original mineral aggregates.

Volumetric properties (e.g., $V_a$, VMA, VFA) of the mixture were determined using theoretical maximum specific gravity ($G_{mm}$) by ASTM D2041 (2011) and bulk specific gravity ($G_{mb}$) by ASTM D6752 (2018) using the CoreLok® device. Additionally, ASTM C1252 Method A (2017) angularity was also measured on the final aggregate blend including steel aggregates.

The most notable deviation from typical Superpave mix design practices was that specimen mix masses were reduced to target 75 mm tall specimens (150 mm diameter) rather than the typical 115 mm tall specimens. This was done in order to later use these specimens for Asphalt Pavement Analyzer (APA) testing under AASHTO T340 [2010]), though this testing was ultimately not performed due to equipment issues at the time. It should be noted that sawing 115 mm tall specimens to 75 mm was not considered an appropriate option due to the difficulty in sawing iHMA specimens containing steel (discussed in Section 6.4). Differences between mix designs performed using 75 mm versus 115 mm tall specimens are

possible due to density gradients developed in gyratory compacted specimens; however, the differences should not be meaningful.

### 4.2.4 Field patching methods

This section describes field patching procedures from the time asphalt, either HMA or iHMA, was passed to the patching team. Figure 4.11 provides an overview of the patching process. Figure 4.11a illustrates iHMA temperature after heating, showing the mix reached about 320°F.

Figure 4.11. Overview of field patching method.

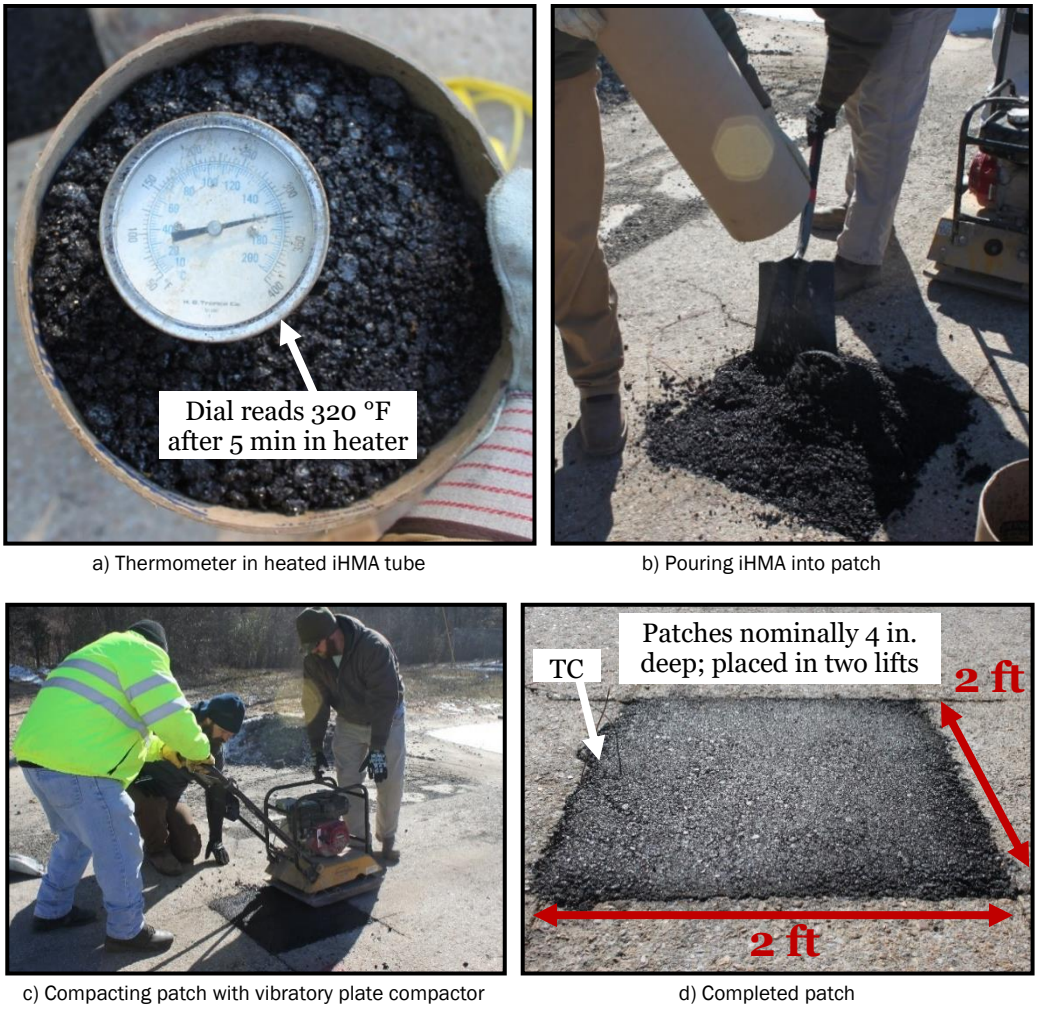


a) Thermometer in heated iHMA tube

b) Pouring iHMA into patch

c) Compacting patch with vibratory plate compactor

d) Completed patch

Each iHMA tube was poured into a patch (Figure 4.11b) and spread evenly with square-nose shovels. Compaction was performed with several passes of the vibratory plate compactor (Figure 4.11c). Typically, one operator guided the compactor while another pushed down on it to provide confinement so that more of its energy was imparted into the mix. Figure

4.11d shows a completed patch. With the exception of the heating method, the placement and compaction method was identical regardless of mix type (iHMA or HMA). HMA (AC2) was transported from laboratory ovens to the test site immediately before use so that it maintained temperature.

HMA and iHMA patches were placed in two lifts with each lift requiring about one 5-gal bucket of mix. Placement and compaction methods were the same whether it was the first or second lift. The only real distinction between the two was that operation of the plate compactor was slightly more difficult for the first lift since the compactor could not ride smoothly on and off the patch. In between the two lifts, a single thermocouple was placed with its tip located in the center of the patch.

### 4.2.5 Field data collection

Data collected in field testing included patching times, ambient and patch temperatures, rutting under simulated F-15E traffic, in-place density, and visual monitoring over time. Patch temperatures were monitored using thermocouples embedded in the center of each patch as described in the previous section and using the equipment described in Section 4.2.2.

Figure 4.12 provides photographs related to rutting measurements. ERDC's F-15E load cart (Figure 4.12a) was used to apply simulated traffic using standard loading conditions of 35,235 lb on a single 325 psi F-15E tire. Traffic was applied 2 hr after patching. Because of the tire width relative to the size of each patch, channelized traffic was applied rather than the more typical normally distributed traffic pattern used for simulated trafficking.

Figure 4.12. Field trafficking.

a) F-15E load cart b) Typical rut profile

Rutting criterion established for this project was 1 in. (25 mm) or less after 100 passes beginning at 2 hr. Figure 4.12b shows a typical rut profile with a straightedge placed across the rut in the transverse direction. The figure shows a folding rule; however, actual measurements were obtained using digital calipers. Rut depths measured across the rut (as in Figure 4.12b) also accounted for any upheaval beside the rut; this rut depth is hereafter referred to as total rut depth. Rut depths in the longitudinal direction along the wheel path (i.e., does not account for upheaval) were also measured for comparison.

In-place density was measured on cores cut from some patches. Cores were sliced to a thickness of 75 mm (3 in.) using a diamond-blade masonry saw in order to remove the irregular bottom faces. $G_{mb}$ was measured via ASTM D6752 (2018), and $V_a$ was calculated using mix design $G_{mm}$.

Patches are being visually monitored on a periodic basis where the primary item of interest is patch deterioration due to environmental distresses. In particular for iHMA, evaluating the steel aggregate is of interest. Steel that is exposed (such as surface steel particles that had the binder film worn off during trafficking) is expected to rust like any steel material would. The questions are: To what degree does the steel rust, and to what degree does it impact the patch long term?

## 4.3 Test plan

### 4.3.1 Laboratory testing

Laboratory testing can be broken into two phases. The first phase investigated induction heating of mixes with steel aggregates and consisted of two experiments, which are detailed in Table 4.1. The second phase established an iHMA mix through a typical Superpave volumetric mix design process following the method described in Section 4.2.3. The iHMA mix was then used for field testing.

Table 4.1 describes the two laboratory experiments conducted where steel content (Experiment 1) and particle size and type (Experiment 2) were evaluated for heating properties. The materials tested were mineral and steel aggregates only; asphalt binder was not added. This was primarily done to facilitate efficient testing as more testing could be accomplished in a shorter time with less material. This was deemed acceptable since there should not be any meaningful interaction between asphalt binder and

steel. All materials, both mineral and steel aggregates, were fractionated for controlled batching, batched, and mixed thoroughly before testing.

Table 4.1. Test plan for laboratory heating experiments.

| Steel Size | Test No. | ID | Reps | Heat Time (min) | Temp Meas. Method | Volume Replacement Percentage (%) | | | | | |
|---|---|---|---|---|---|---|---|---|---|---|---|
| | | | | | | Size 1 Steel | | | | Size 2 Steel | |
| | | | | | | B | CS | CW | G | CW | G |
| Experiment 1 – Varying Volume Replacement, Fixed Steel Type | | | | | | | | | | | |
| Size 1 & 2 Blends | 1 | 5% VR | 1 | 20 | IR | — | — | 2.5 | — | 2.5 | — |
| | 2 | 10% VR | 1 | 20 | IR | — | — | 5.0 | — | 5.0 | — |
| | 3 | 15% VR | 4 | 6-8, 20 | IR | — | — | 7.5 | — | 7.5 | — |
| Experiment 2 – Varying Steel Type, Fixed Volume Replacement | | | | | | | | | | | |
| Size 1 Only | 1 | 15B - 0 | 3 | 3.5 | TC | 15 | — | — | — | — | — |
| | 2 | 15CS - 0 | 3 | 3.5 | TC | — | 15 | — | — | — | — |
| | 3 | 15CW - 0 | 3 | 3.5 | TC | — | — | 15 | — | — | — |
| | 4 | 15G - 0 | 3 | 3.5 | TC | — | — | — | 15 | — | — |
| Size 1 & 2 Blends | 5 | 7.5B - 7.5CW | 3 | 3.5 | TC | 7.5 | — | — | — | 7.5 | — |
| | 6 | 7.5B - 7.5G | 3 | 3.5 | TC | 7.5 | — | — | — | — | 7.5 |
| | 7 | 7.5CS - 7.5CW | 3 | 3.5 | TC | — | 7.5 | — | — | 7.5 | — |
| | 8 | 7.5CS - 7.5G | 3 | 3.5 | TC | — | 7.5 | — | — | — | 7.5 |
| | 9 | 7.5CW - 7.5CW | 3 | 3.5 | TC | — | — | 7.5 | — | 7.5 | — |
| | 10 | 7.5CW - 7.5G | 3 | 3.5 | TC | — | — | 7.5 | — | — | 7.5 |
| | 11 | 7.5G - 7.5CW | 3 | 3.5 | TC | — | — | — | 7.5 | 7.5 | — |
| | 12 | 7.5G - 7.5G | 3 | 3.5 | TC | — | — | — | 7.5 | — | 7.5 |
| Size 2 Only | 13 | 0 - 15CW | 3 | 3.5 | TC | — | — | — | — | 15 | — |
| | 14 | 0 - 15G | 3 | 3.5 | TC | — | — | — | — | — | 15 |

*– Experiment 1 tested blends in a 3 gal container; Experiment 2 tested blends in a 1 gal container.*
*– Temperature measurement methods were via infrared camera (IR) or thermocouple probe (TC).*

As shown in Table 4.1, steel aggregate content was defined on a volume replacement (VR) basis rather than a mass basis. This allowed steel aggregates to replace mineral aggregates with minimal impact to bulk gradation. Replacement on a mass basis would not be straightforward due to the large $G_{sb}$ differences between mineral and steel aggregates. This distinction is discussed further in Section 5.3.

To batch materials for each Table 4.1 test sample, the AC1 aggregate gradation (Table 3.1) was batched less the mass corresponding to the VR (e.g., 10%). Following the Table 3.3 gradations, the mass of steel corresponding to the VR was then batched. All materials were thoroughly mixed in a bucket mixer, then transferred to the heating container.

The goal of Experiment 1 was to evaluate effects of steel content on induction heating ability to determine the amount of steel required to achieve hot mix temperatures in several minutes. The goal of Experiment

2 was to use the selected VR value for multiple combinations of all steel materials tested. This included both different steel types (e.g., B versus CW) and different steel sizes (e.g., Size 1 versus Size 2).

### 4.3.2 Field testing

Field testing in this project occurred 18 January 2018 at ERDC's Outdoor Pavements Test Facility in Vicksburg. Testing was conducted in an asphalt test section that had been in place for several years. Figure 4.13 provides an overview of the testing layout where nine total 2 by 2 ft patching repairs were completed. Asphalt thickness was approximately 4 in. over a well-graded limestone base.

Figure 4.13. Field testing layout at the ERDC Outdoor Pavements Test Facility.

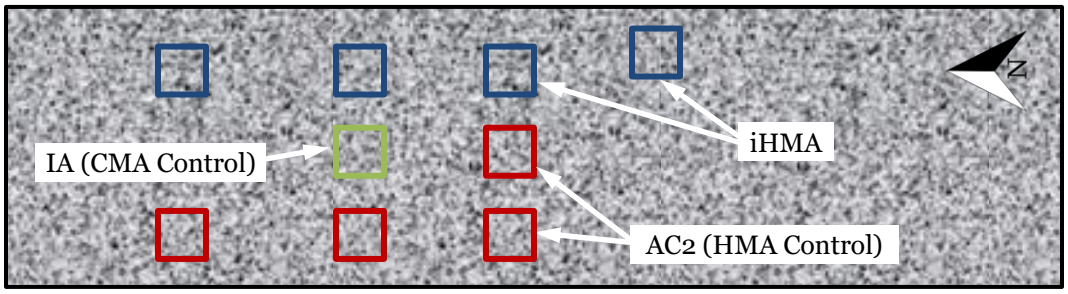


a) Illustration of testing layout

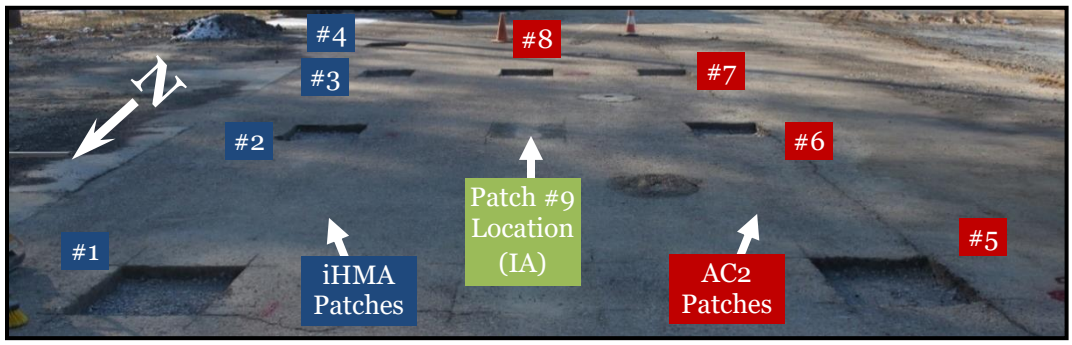


b) Photograph of testing layout showing patch IDs

Patches 1 to 4 were iHMA, patches 5 to 8 were AC2 (HMA control), and patch 9 was IA (proprietary CMA control). Note the IA patch was placed for a different purpose at a later date after the original field test; however, it was ultimately trafficked for an additional comparison. For iHMA and AC2, three patches (Patches 1 to 3 or 5 to 7, respectively) were trafficked while the fourth (Patch 4 or 8, respectively) was cored for in-place density.

Prior to patch installation, additional limestone base material was added and compacted using the vibratory plate compactor in order to level the

patches. Nominal patch depths were 4 in.; actual depth measurements after leveling with limestone base ranged from 3.25 to 3.5 in.

# 5 Laboratory Results

## 5.1 Effects of steel volume replacement

This section provides results relating to Experiment 1 in Table 4.1 of Section 4.3.1. Figure 5.1 illustrates the typical heating progression observed for each blend tested. The infrared camera identified the maximum temperature, reporting it in the top left corner of each image.

Figure 5.1. Example Infrared Images for Experiment 1 (10% VR).

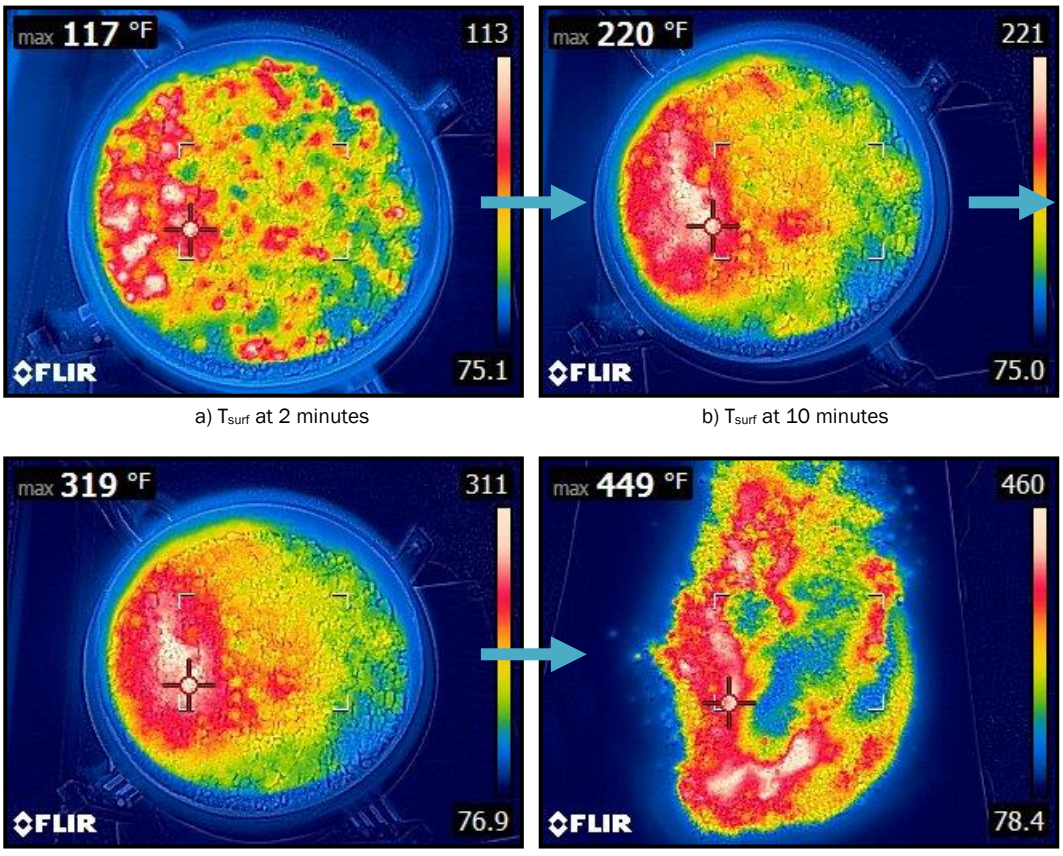


a) $T_{surf}$ at 2 minutes

b) $T_{surf}$ at 10 minutes

c) $T_{surf}$ at 20 min

d) Mix Spread Out to Measure $T_{int}$ at 20 min

As highlighted by Figure 5.1, there are several deficiencies with infrared (IR) measurements. First, IR measures maximum surface temperature, not average temperature. Even on the surface, temperatures vary considerably. This was generally due to the dispersion of steel at the surface; in transferring blended material from the mixing bucket to the heating container, the last little bit of material (i.e., the material on the surface in Figure 5.1) tends to segregate due to the mass differences. This segregation appeared to be only near the surface, meaning it would not have a meaningful effect on the heating of the majority of mix.

In addition to the surface temperature variability, surface temperatures ($T_{surf}$) were considerably different from internal temperatures ($T_{int}$). This can be seen by comparing the max temperatures of 319 and 449°F in Figures 5.1c and 5.1d, respectively. This behavior was not unexpected as the surface is exposed to air and will cool at a faster rate and because the plane at which the surface lies is near the top of the induction coil (more energy will be absorbed by material well inside the coil).

Given these issues, an explanation for the use of IR measurements is warranted. At the time, it had not yet been determined that TC measurements would provide valid, reliable temperatures (i.e., that the TC would not be self-heated by the induction current). Early trials with TC measurements using a small, hand-held data logger reported errors when trying to measure $T_{int}$ during heating. It was initially thought that the TC was self-heating beyond the data logger's useable range, causing errors. Later discussions with Ambrell indicated small-wire-diameter TCs can effectively be used with minimal self-heating effects, but the acquisition system must have sufficient shielding to isolate it from induction current effects. This proved to be the issue with the small, hand-held data logger, which was resolved with the Campbell Scientific data acquisition described in Section 4.2.2. Ultimately, IR measurements provided an initial starting point, and TC measurements were used for Experiment 2.

Figure 5.2 plots temperature versus heating time curves for all Experiment 1 blends. The first three tests for 5, 10, and 15% VR were performed for 20 min, and $T_{surf}$ was measured every 2 min. As mentioned previously, final 20-min $T_{surf}$ and $T_{int}$ values differ considerably.

Figure 5.2. Temperature versus heating time for varying steel VR (Experiment 1).

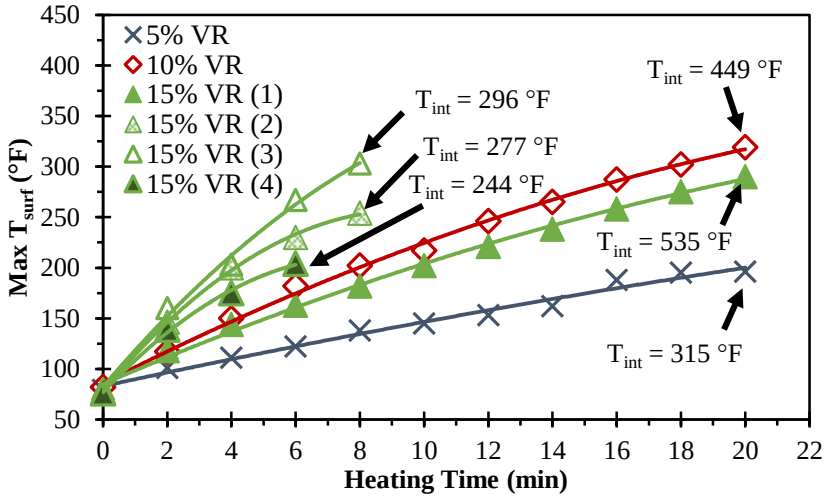

There was a noticeable increase in heating ability from 5 to 10% VR; however, it is interested that 15% VR exhibited lower temperatures than 10% VR. This again highlights an issue with $T_{surf}$ measurements where the measurement is highly dependent on how many steel particles happen to lay on the surface.

$T_{int}$ measurements were much more representative and showed progressive increases in temperature from 5 to 10 to 15% VR as would be expected. Additionally, all VRs exceeded 300°F $T_{int}$ after 20 min, with 15% VR reaching well over 500°F, at which point safety would become a much greater concern (i.e., temperatures are reaching asphalt binder flash point temperatures). While 5% VR reached 315°F, it required essentially a full 20 min to do so, well exceeding target times in this project.

In order to determine $T_{int}$ at earlier heating times, additional replicates with 15% VR were heated for 6 to 8 min. $T_{int}$ measured 244°F after 6 min and 277 to 296°F after 8 min. These temperatures were close to or exceeded the threshold criteria of 250°F but did not exceed the objective criteria of 300°F. At this point in the project, results were discussed with Ambrell engineers who felt that the LIH could be adjusted slightly to improve heating in order to exceed 300°F in fewer than 8 min with 15% VR. As a result of this discussion, LIH adjustments were applied for Experiment 2, and 15% VR was ultimately selected as an appropriate steel content for further iHMA feasibility testing.

## 5.2 Effects of steel type and size

This section provides results relating to Experiment 2 in Table 4.1 of Section 4.3.1. Figure 5.3 illustrates typical temperature versus time curves for four TCs inserted into the center of the mix at different depths as discussed in Section 4.2.2. For the 1 gal container used in Experiment 2, $TC_6$ (TC at 6 in.) was located right at the mix surface, and $TC_8$ (TC at 8 in.) was in air above the mix surface. For analysis, $TC_4$ (TC at 4 in.) was evaluated as it was closest to the center of the mix.

For the combination of LIH settings, 1 gal container size, and materials used, several preliminary trials indicated temperatures around or well over the 300°F objective temperature could be reached in 3.5 min. These tests, though not shown, were conducted similarly to all others in Experiment 2. Ultimately, a 3.5 min heating time was selected.

Figure 5.3. Example heating curves for Experiment 2.

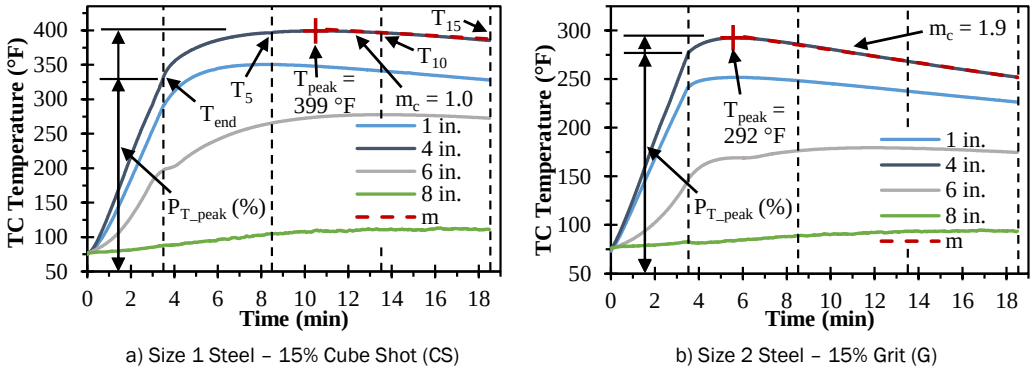


a) Size 1 Steel – 15% Cube Shot (CS)

b) Size 2 Steel – 15% Grit (G)

As indicated in Figure 5.3, a number of variables were reported. $T_{int}$ values were reported at the end of the 3.5 min heating cycle ($T_{end}$) and at 5, 10, and 15 min after the heating cycle ended ($T_5$, $T_{10}$, and $T_{15}$, respectively). Peak temperature ($T_{peak}$) was also reported.

Percent of peak temperature ($P_{T\_peak}$) was defined as the ratio of $T_{end}$ to $T_{peak}$ expressed as a percentage. It was used as an indicator of how much of the total mix temperature gain was achieved during the heating cycle versus how much of the total mix temperature gain was achieved after heating due to continued heat dispersion from steel aggregates. Lastly, post-peak cooling slope ($m_c$) was also calculated.

Figure 5.3 illustrates typical differences between Size 1 and Size 2 steel aggregates. For example, $P_{T\_peak}$ was lower for the larger Size 1 CS than Size 2 G. Figure 5.3a shows the Size 1 CS blend gains almost an additional 75°F through over 7 min after the heating cycle ended; in contrast, Figure 5.3b shows the Size 2 G blend gained less than 25°F after the heating cycle.

While induction currents heat the steel particles almost instantaneously, the bulk mixture temperature lags behind as heat in the steel is dispersed into surrounding aggregates and throughout the mix. As illustrated by Figure 5.3, larger steel particles (i.e., Size 1) have more mass and dissipate heat at a slower rate than smaller Size 2 particles. In some aspects, this behavior is desirable from an iHMA mix because it does not begin cooling immediately once the induction heater is turned off. This helps the mix remain at high temperatures longer, allowing more useable time for placement. However, there is a practical limit; if the mix required an additional 10 min after heating to reach $T_{peak}$, the value of the short heating time is negated to some extent. In contrast, smaller Size 2 particles

dissipate temperature quickly, meaning the bulk mix temperature will peak and then drop sooner.

In a similar manner, steel size also affects cooling rate. For example, $m_c$ in Figure 5.3 shows that the Size 2 G blend cools about twice as fast as the Size 1 CS blend. Ultimately, the $m_c$ parameter was abandoned in favor of $P_{T\_peak}$ because $P_{T\_peak}$ was found to be more repeatable and informative overall. For example, coefficient of variation (COV) for $m_c$ ranged from 3 to 91% and averaged 34%, whereas $P_{T\_peak}$ COV ranged from 1 to 18% and averaged 14%.

Figure 5.4 summarizes all Experiment 2 results. Regarding particle size, Size 1 steels, at 422°F on average, returned the highest peak temperature followed by the Size 1 & 2 blends (405°F on average) and the Size 2 steels (336°F on average). However, Size 1 steels yielded the lowest $P_{T\_peak}$ values (83% on average), whereas Size 2 steels yielded 92% $P_{T\_peak}$ on average for comparison. This tradeoff in $T_{peak}$ and $P_{T\_peak}$ suggest use of both Size 1 and Size 2 steels would offer the best balance for a general-use iHMA mix. Though not relevant to heating ability, a steel blend is also preferred for mix design because replacing 15% well-graded aggregate with a single steel size (e.g., CS) could not be done without dramatically affecting gradation.

Figure 5.4. Effect of steel type and size for 15% VR (Experiment 2).

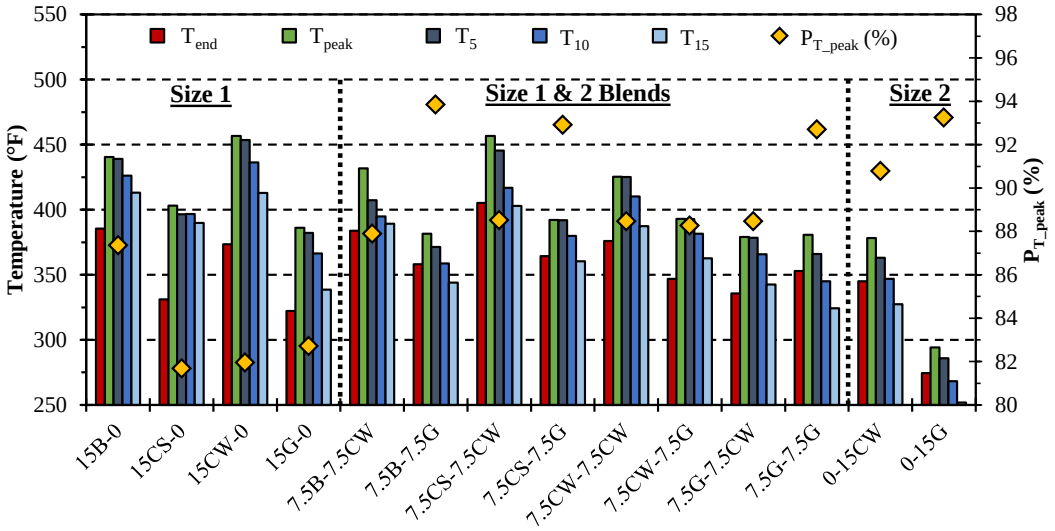


Regarding steel type, it is quite apparent from Figure 5.4 that heating ability varies from one steel type to another. For example, CW heats considerably better than G for either Size 1 or Size 2 particles. Whether this is due to differing steel compositions, particle shapes, or some other reason is

unknown. It should be noted that variability among the three replicate measurements did not appear to be a significant contributing factor. For example, $T_{peak}$ COV average 7% and ranged from 0 to 17% overall. Explaining the effect of steel type likely requires a more theoretical assessment; considering initial proof of concept was the primary focus herein, more theoretical assessments were not of great interest to this project.

Heat retention through 15 min of cooling varied by steel size and type. The 15CS-0 blend retained heat the best, dropping only 13°F from $T_{peak}$ to $T_{15}$. Heat retention was worst for 7.5G-7.5G, which dropped 56°F, though this is not entirely unmanageable considering the blend started at a $T_{peak}$ of 381°F, which is well over the 300°F objective temperature.

With regards to selecting the most ideal blend for iHMA mix design, $T_{peak}$ ranged from 294°F for 0-15G to 457°F for 15CW-0 or 7.5CS-7.5CW with every other blend option in between comfortably meeting the 300°F objective target. Considering all of these results were obtained with only a 3.5 min heating cycle, this work appears promising for full-scale iHMA. However, it is important to recognize that although the general trends (e.g., $P_{T\_peak}$ is lower for Size 1 than Size 2 steels) would likely carry over from the LIH to the full-scale FIH, the actual temperature values would probably not carry over.

The main focus of this project has been on the feasibility of induction heating for yielding hot mix temperatures. Within that goal, the assumption has been made that it may be difficult to meet 250 or 300°F, which also implies a primary focus on minimum temperature. It is important to note that, although a maximum temperature was not explicitly discussed, higher temperature is not always better. Many of the Figure 5.4 temperatures approach or exceed flash point specifications for asphalt binder. For full-scale iHMA work (when binder is added), these high temperatures would pose serious safety concerns.

Results presented in this section, as well as the previous section, demonstrate that heating properties of iHMA mixes can be tailored to some degree by adjusting variables such as steel type, size, and VR. This creates potential opportunities for different types of iHMA to be developed. For example, a large-patch iHMA might utilize Size 1 CS to help retain heat longer so that a number of iHMA tubes could be heated successively and held until enough tubes were ready for the repair in

question. While this potential for creating repair-specific mixes exists, this type of refinement was considered beyond the scope of the project.

For the purposes of this project where initial feasibility was the focus, a general purpose mix with relatively balanced heating properties was of interest. As a result, the 7.5CS-7.5G blend was selected for mix design and field testing. It exhibited a high $P_{T\_peak}$ value (93%), middle of the road temperatures (e.g., $T_{peak}$ of 392°F), and reasonable heat retention (32°F total drop from $T_{peak}$ to $T_{15}$). An additional factor was that it used the two most angular steel materials (CS and G), which would be preferable with respect to stability and rutting performance.

## 5.3 Volumetric mix design

Based on findings presented in Sections 5.1 and 5.2, the 7.5CS-7.5G steel blend (total volume replacement of 15%) was selected for a formal mix design process. The process began by using a gradation blending spreadsheet in an effort to recreate the AC1 gradation as closely as possible while also incorporating 7.5% CS and 7.5% G. This was considered the starting point for mix design and was accomplished primarily by reducing the amounts of crushed gravel and RAP, with slight reductions in limestone and sand contents.

Trial batches with the first gradation blend were quite different from the original AC1 design in terms of volumetric properties. This was not entirely unexpected considering the drastic differences in $G_{sb}$ values, which would affect mass-volume relationships, the increased angularity of the steel, and the reduction in fines that occurred by replacing mineral aggregate with steel. Several additional trial batches were prepared to investigate these issues. As with any mix design, it is an iterative process, probably to a greater extent in this case given the unique characteristics of an asphalt mix with this type of steel aggregate.

Ultimately, the blend shown in Table 5.1 and Figure 5.5 was selected. The key aspect of the final iHMA blend was that approximately 0.5% additional hydrated lime was added to replace the dust content lost when mineral aggregate was removed to make room for the steel aggregate.

When working with AC1 based on the mix design gradation and blend, which is by mass, the volume-based aggregate percentages in Table 5.1 are obtained, resulting in a slightly different actual gradation by volume. This

volume-based AC1 gradation was the target for the iHMA gradation, which Table 5.1 shows as fairly similar to AC1. For iHMA batching purposes, the volume-based stockpile percentages were converted to a mass basis.

Table 5.1. Mix design property comparison for AC1 and iHMA.

| Mix Designation | | AC1 | | iHMA | |
|---|---|---|---|---|---|
| $P_b$ (%) | | 5.9 | | 5.0 | |
| $P_{be}$ (%) | | 5.1 | | 4.2 | |
| $P_{ba,\,mix}$ (%) | | 0.8 | | 0.8 | |
| $V_{be}$ (%) | | 11.4 | | 11.8 | |
| $G_{mm}$ | | 2.385 | | 2.987 | |
| $G_{sb}$ | | 2.547 | | 3.233 | |
| $G_{se}$ | | 2.600 | | 3.320 | |
| $G_{sa}$ | | 2.646 | | 3.387 | |
| FAA | | 44.1 | | $41.3_{(A)}$, $25.9_{(C)}$ | |
| VMA (%) | | 15.4 | | 15.8 | |
| VFA (%) | | 74.0 | | 74.0 | |
| $P_{200}/P_{be}$ Ratio | | 0.97 | | 1.21 | |
| | | Mass Basis | Volume Basis | Mass Basis | Volume Basis |
| Percent Passing (%) | 1.0 in. / 25.0 mm | 100 | 100 | — | 100 |
| | 3/4 in. / 19.0 mm | 100 | 100 | — | 100 |
| | 1/2 in. / 12.5 mm | 100 | 100 | — | 100 |
| | 3.8 in. / 9.5 mm | 94 | 94 | — | 95 |
| | #4 / 4.75 mm | 61 | 64 | — | 70 |
| | #8 / 2.36 mm | 40 | 40 | — | 41 |
| | #16 / 1.18 mm | 29 | 29 | — | 30 |
| | #30 / 0.60 mm | 21 | 21 | — | 21 |
| | #50 / 0.30 mm | 10 | 11 | — | 12 |
| | #100 / 0.15 mm | 7 | 7 | — | 7 |
| | #200 / 0.075 mm | 4.9 | 5.1 | — | 5.1 |
| 1/2 in. Crushed Gravel (%) | | 62 | 61.4 | 39.7 | 52 |
| #11 Limestone (%) | | 7 | 6.6 | 8.0 | 10 |
| Coarse Sand (%) | | 10 | 9.4 | 5.2 | 6.5 |
| RAP (%) | | 20 | 21.5 | 10.5 | 15 |
| Hydrated Lime (%) | | 1 | 1.1 | 1.1 | 1.5 |
| Size 1 CS (%) | | 0 | 0 | 18.1 | 7.5 |
| Size 2 G (%) | | 0 | 0 | 17.4 | 7.5 |

*-- ASTM C1252 FAA method (2017) denoted by subscript (A) or (C) for Method A or C, respectively.*
*-- AC1 mix design gradation was performed on a mass basis. If AC1 is batched according to the job mix formula (JMF, by mass), the resulting volume-based gradation and JMF would be produced.*
*-- Since all iHMA work was done directly on a volume basis, there is no mass-based gradation to report. However, for batching the JMF, volume-based blend percentages were converted to masses.*

Figure 5.5. iHMA design gradation (compared to AC1 on a volume basis).

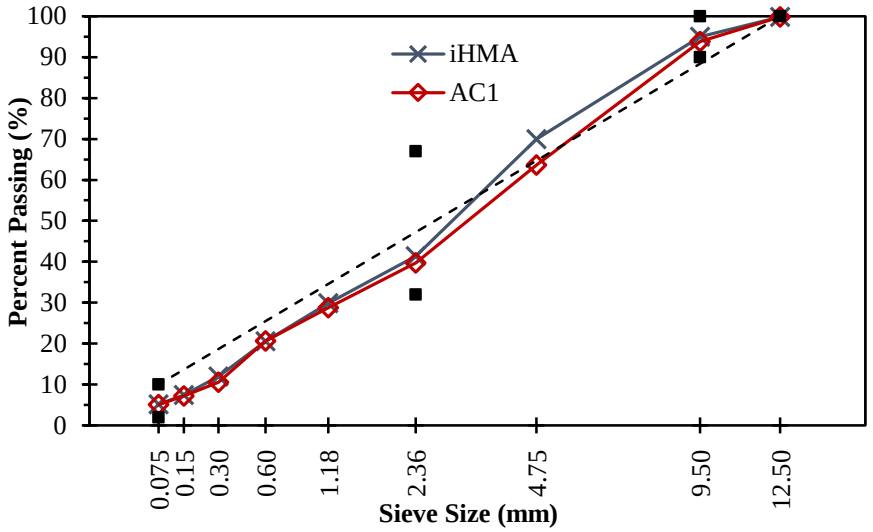


This conversion back and forth between mass and volume basis illustrates the importance of distinguishing the two. Gradation blending is typically thought of on a mass basis for convenience, which generally does not amount to much practical difference for conventional mixes as shown with AC1 in Table 5.1. The $G_{sb}$'s of mineral aggregates are similar enough that the error induced when blending by mass is not meaningful, particularly in relation to the degree in which an asphalt plant can be controlled. More correctly, however, blending is technically a volume-based activity that seeks to achieve the various volumetric sizes required in the produced mix. With steel $G_{sb}$'s being about three times higher, gradation blending must be done on a volume basis, with volumes being converted by $G_{sb}$ to masses for batching. Blend percentages for iHMA illustrate this point; 52% crushed gravel by volume is only 39.7% by mass, whereas 15% steel by volume (7.5% CS plus 7.5% G) is 35.5% by mass.

Table 5.1 reports iHMA blend FAA values for Methods A and C. For Method A, which tests #8 to #100 size material (meaning CS was not included), an FAA value of 41.3 was obtained. This value was slightly, though not detrimentally, lower than that of the original AC1 value. For Method C, which tests all minus #4 material (meaning CS was included), FAA dropped considerably to 25.9. Just like the CS FAA value in Table 3.3, this value was not believable based on the visual angularity of CS. For the Table 3.3 value, it was discussed in Section 3.3 that CS was angular to the point it would not flow through the C1252 funnel. In this case with the entire iHMA blend, similar attempts to stir the funnel's contents did encourage material to flow through; however, it only encouraged the finer

materials, not the CS. This meant that the finer materials filled the brass measure first, followed by the CS, which probably collapsed the void structure to some extent and would reduce FAA. Ultimately, FAA based on Method C appears invalid.

Figure 5.6 visually illustrates mix design results for the Figure 5.5 iHMA blend. The design binder content ($P_{b,des}$) at 4% $V_a$ equaled 5.0%. While this is about 1% lower than the AC1 $P_b$ in Table 5.1, this direct comparison cannot be made since $P_b$ is mass-based. Effective binder volume ($V_{be}$) is a more appropriate parameter, in which case the iHMA value of 11.8% is just slightly higher than that of AC1 at 11.4%. This difference is a result of the increase in VMA from the AC1 mix to iHMA. The change in VMA is relatively small and not unexpected considering the slightly different gradation and particle shape.

Figure 5.6. iHMA volumetric mix design relationships.

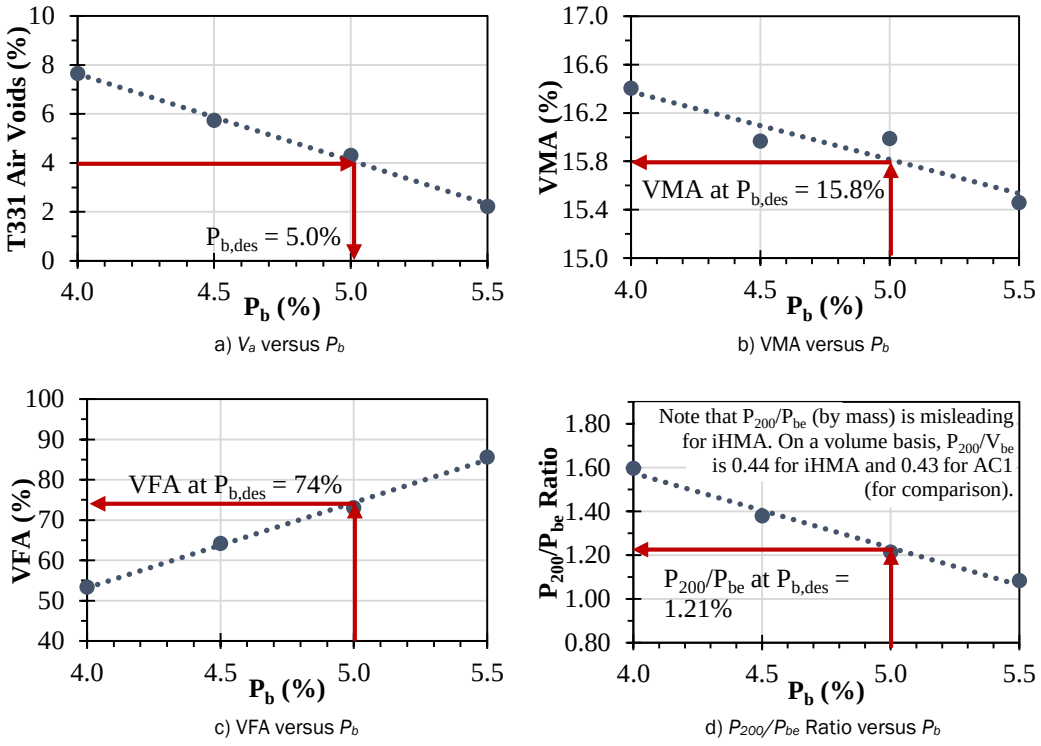


The mix design reported in this section (i.e., Table 5.1) was established as the iHMA mix design used throughout the remainder of the project. This mix was produced in larger batches to fill 5 gal fiber tubes for use in field testing.

# 6 Field Results

Field testing was conducted according to the test plan described in Section 4.3.2 following the method described in Section 4.2.4.

## 6.1 Field test processes, timelines, and temperatures

Figure 6.1 provides a timeline of repairs and trafficking and includes ambient air temperatures and internal patch temperatures. An important point demonstrated in this field evaluation was iHMA's versatility to be used in a cold environment when conventional HMA would be unavailable. Air temperatures were essentially at freezing or below for the entire duration of the field test. It should be noted, however, that iHMA tubes had been in the laboratory with all the other tools and supplies the night before the field evaluation. Supplies and materials were staged outside approximately 2 hr before repair work began, meaning the iHMA itself would not have been at ambient outdoor temperature. Determining how well iHMA would heat from below-freezing temperatures would warrant additional testing. In the absence of additional testing at present, heating rates in Figure 5.3 were essentially linear, which indicates based on field heating performance that heating iHMA from below freezing would require 1 min of additional heating time (i.e., 6 min instead of 5). At the very least, performing the work in below-freezing temperatures demonstrates the feasibility of all other tasks (e.g., compaction).

Figure 6.1. Overview of field test timing and temperatures.

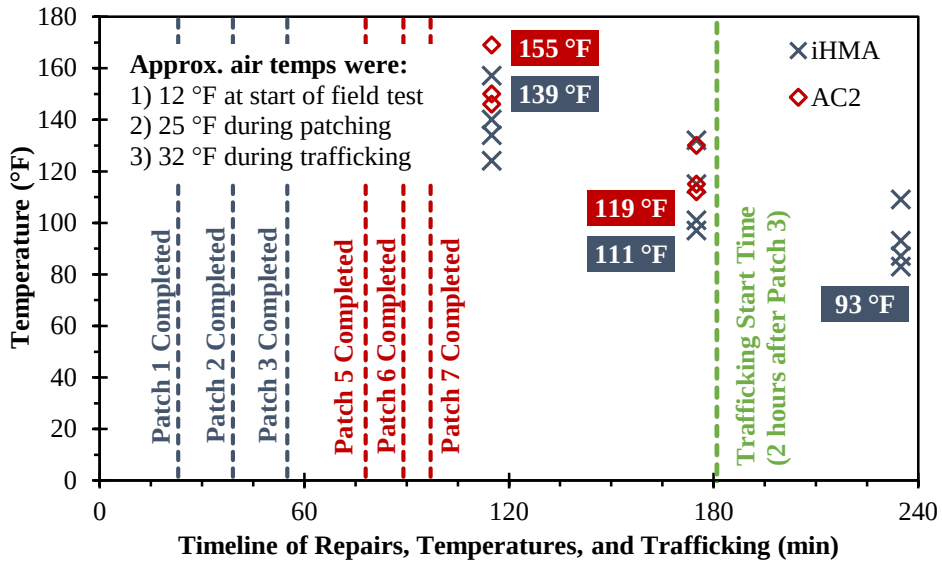

Regarding the repair team, the process seemed to work well with one dedicated FIH operator, two dedicated patching operators, and one runner that shifted between helping the FIH operator load or unload the FIH and helping the patching team. The FIH operator oversaw the FIH and monitored the patching crew to ensure iHMA tubes were heated as needed. In previous indoor trials with the FIH, a 4 min heating cycle yielded approximately 320°F; however, due to the cold weather, it was found that a 5 min heating cycle was more appropriate and easily achieved 320°F (refer back to dial thermometer in Figure 4.11a).

As iHMA was heated, the FIH operator or runner passed it to the repair team who poured it into a patch, leveled it with a shovel, and then compacted it as described in Section 4.2.4. Completed 2 ft by 2 ft by 3.5 in. (nominal) patches required about 2.25 iHMA tubes each. Thus, it required approximately 11.25 gal of loose iHMA to yield approximately 8.75 gal of compacted iHMA in a completed patch. This corresponds to a yield factor of 75 to 80%.

Referring to Figure 6.1, iHMA repairs required from 13 to 23 min each (including the untrafficked Patch 4), while AC2 repairs required 6 to 11 min each (including the untrafficked Patch 8). One reason that AC2 repairs were faster was that the step of heating the material was essentially omitted as far as the timing data is concerned because AC2 was heated beforehand. While heating the materials will undoubtedly add to the repair time to some degree, it is also believed that iHMA repairs were slower because they were conducted first, meaning the "learning curve penalty" was applied to iHMA repairs more so than AC2 repairs. It could be argued the learning curve is not very steep with these small repairs; however, it did take a little time for the team to refine its process, particularly for added steps that would not normally be included (like thermocouple installation).

Again referring to Figure 6.1, patch temperatures could not be continuously recorded due to data acquisition limitations, but they were measured at times corresponding to approximately 1, 2, and 3 hr after iHMA Patch 3 was placed. For comparison, these times corresponded to halfway between placement and trafficking, right before trafficking, and right after trafficking (all for iHMA). At these times, internal iHMA patch temperatures averaged 139, 111, and 93°F, respectively. AC2 temperatures were measured at the same time intervals and were slightly higher than

iHMA temperatures since these times corresponded to approximately 15 and 75 min after AC2 patch placement.

## 6.2 Field trafficking

During trafficking, the front axle of the F-15E load cart actually broke after 74 passes were applied to the iHMA patches, and further trafficking was postponed. While this was not an ideal choice, there were no other options to continue trafficking.

Following load cart repairs, trafficking was resumed one month later. Relative to the initial test day, ambient temperatures were much warmer at approximately 70°F. However, internal patch temperatures were approximately 81°F on average. Being slightly cooler by about 30°F should, if anything, benefit AC2 rutting relative to iHMA, which was tested at approximately 110°F. Essentially, iHMA, which is of greater interest in this project than AC2, would be put at a disadvantage by being trafficked 2 hr after placement at 111°F. This implies that if iHMA performed similar to AC2 in more adverse conditions, it would probably perform better than AC2 in similar conditions. While comparisons in this document may not be direct due to the differing test conditions, iHMA should not gain an unfair advantage; thus, it was felt that resuming trafficking one month later was valid.

While the load cart was undergoing repairs, Patch 9 was placed using IA for a different purpose. Patching took place one week prior to the follow-up trafficking. Follow-up trafficking applied the final 26 passes to iHMA patches (Patches 1-3), all 100 passes to AC2 patches (Patches 5-7), and all 100 passes to the IA patch (Patch 9).

Figure 6.2 and Table 6.1 provide F-15E rutting data in mm where 1 in. equals 25.4 mm (nominally 25 mm). Note that asphalt rutting data is typically presented in mm. iHMA and AC2 rutted fairly similarly. AC2 results were more variable, but on average, iHMA yielded slightly better rutting results with a 100-pass rut depth ($RD_{100}$) of 23.3 mm compared to 27.8 mm for AC2. Alternatively, iHMA satisfied the 100-pass threshold, while AC2 only provided 80 passes, on average, to failure. Both hot mix materials far surpassed the CMA control (IA), which survived only 8 passes. Figure 6.3 provides typical post-traffic photographs of each mix for visual comparison.

Figure 6.2. Field rutting results under simulated F-15E traffic.

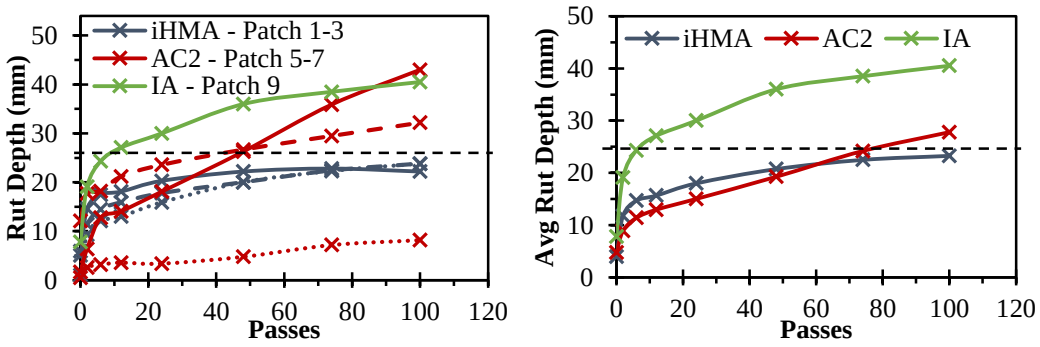


a) Individual Rutting Results

b) Average Rutting Results

While care should be taken in drawing strong conclusions from these field rutting results given the testing issues described, it should be fair to state that iHMA provided rutting resistance at least on par with traditional HMA, and both provided much better rutting resistance than CMA.

Table 6.1. Average field rutting results under simulated F-15E traffic.

| Mix ID | $RD_{100}$ (mm) | $P_{25}$ (passes) |
|---|---|---|
| iHMA | 23.3 | 100 |
| AC2 (HMA Control) | 27.8 | 80 |
| IA (CMA Control) | 40.5 | 8 |

*-- $RD_{100}$ = rut depth (mm) at 100 passes*
*-- $P_{25}$ = number of passes before reaching 25 mm rutting*

Figure 6.3. Representative post-trafficking patch photographs.

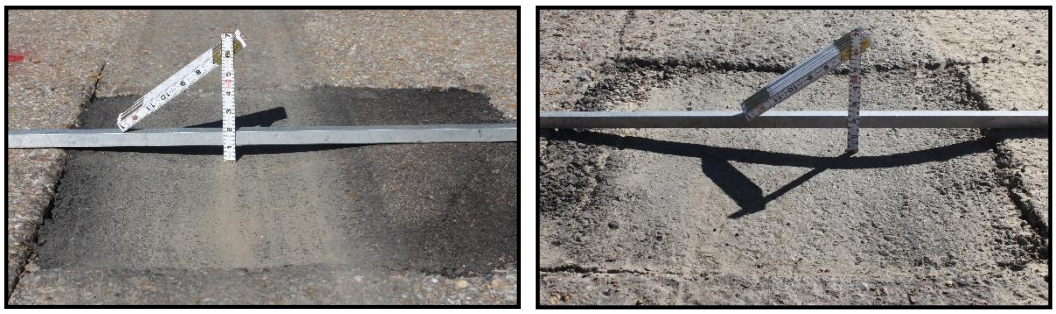

a) iHMA (Patch 3)

b) AC2 – HMA Control (Patch 6)

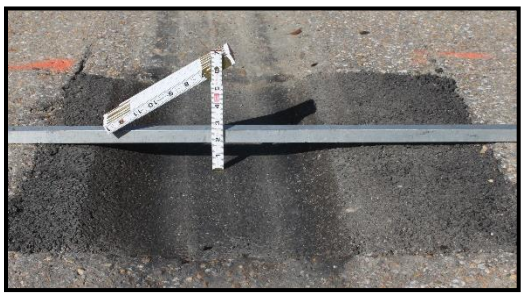

c) IA – CMA Control (Patch 9)

## 6.3 Coring and in-place density

After trafficking, two cores were cut from Patches 4 (iHMA) and 8 (AC2) for in-place density determination. The original test plan intended to cut more cores for laboratory testing of the field-placed materials; it was uncertain as to how easily iHMA cores could be cut and was found to be very difficult.

While coring, steel particles were frequently ripped out of the iHMA mix and thrown into the core bit's cutting path. This caused significant chatter, frequent binding of the bit, and significant wear on the bit (cutting two iHMA cores with a brand new core bit effectively used up its entire cutting life). Once finally cut, these loose steel particles also badly damaged the sides of iHMA cores, making $G_{mb}$ measurement more challenging. However, its effects on $G_{mb}$, if anything, would be adverse.

Cores were then sliced to 75 mm thicknesses using a diamond-blade masonry saw. Though possible, this also proved extremely challenging. Like the core bit, the saw was very ineffective at cutting through iHMA. Unless coring and sawing processes can be improved, this does place limitations on the types of tests that can be performed. If a test requires a specific specimen geometry, the test may not be possible. As far as cutting cores, it is important to remember that patching materials are rarely cored, so this is not a prohibitive issue.

For the four cores that were cut (two iHMA, two AC2), measured $V_a$'s were 6.3 and 9.9%, respectively. For patching purposes, iHMA $V_a$'s were relatively low. AC2 $V_a$'s were quite high, however. This finding may also tie into the faster AC2 repair times as the repair crew may have applied less compaction to AC2 patches in the name of efficiency. Granted, this could be easy to do as patch compaction with a vibratory plate compactor is a somewhat subjective process. It may indicate the need to more carefully draft the wording used in future TTPs that cover this process.

The increased AC2 $V_a$'s relative to iHMA would have definitely had some negative impact on AC2 rutting results, though the actual impact is unknown. This should be taken into consideration when viewing Figure 6.2; however, even if $V_a$'s were accounted for and AC2 rutting were to decrease to less than that of iHMA, the two materials would likely still provide rutting resistance in the general range of the other. This also does not change the fact that iHMA did pass the selected criteria of less than 1 in. (25 mm) of rutting in 100 F-15E passes at 2 hr.

## 6.4 Visual monitoring

The iHMA patches were left in place and have been periodically inspected for longer-term durability or deterioration with exposure to environmental distresses. Probably the biggest issue of concern was the potential rusting of steel aggregates.

Figure 6.4 provides a representative iHMA patch photograph showing its intact condition six months after placement (July 2018). The rut depression from trafficking filled in with dust and silt over time, but the integrity of the patch appears sound. Slight rusting of steel particles is visible on the surface (Figure 6.4b); however, this does not appear to have led to any visible particle loss or raveling to date.

Figure 6.4. Representative iHMA patch 6 months after placement.

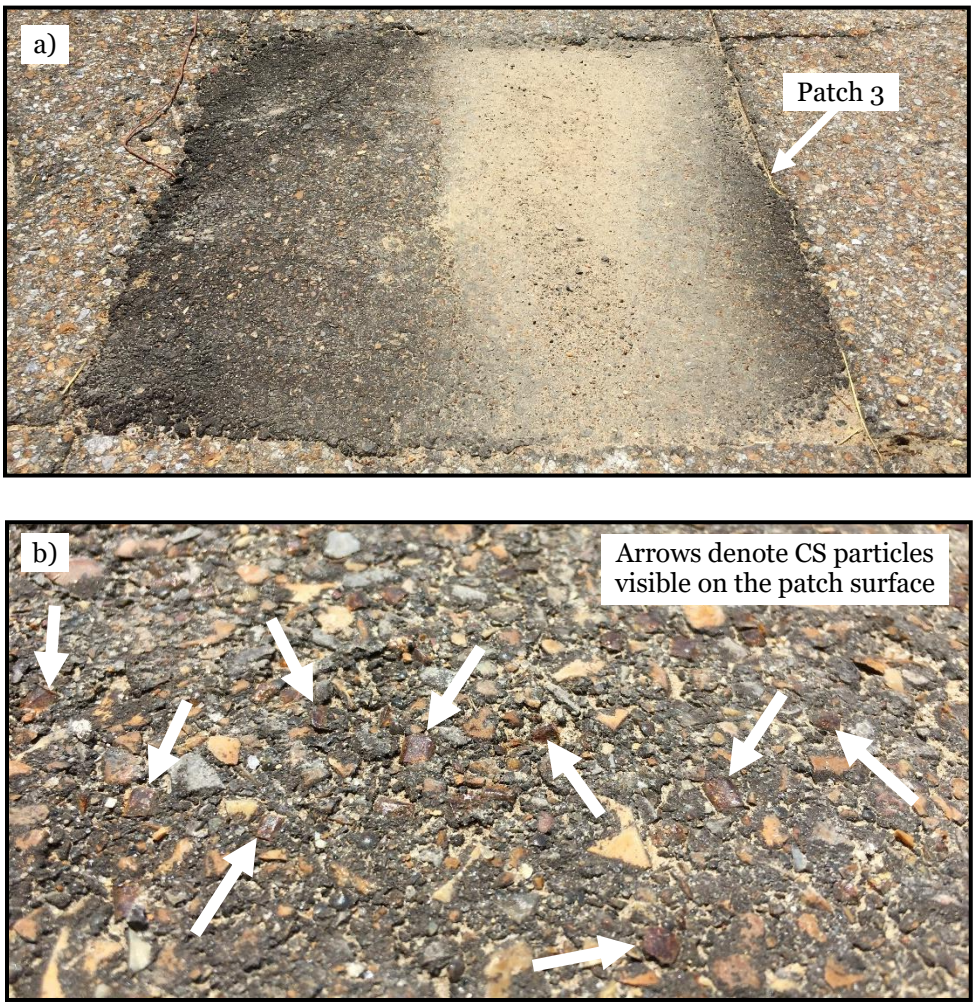

# 7 Discussion of Results

Results presented in this report demonstrated that commercially available steel materials can feasibly be incorporated as steel aggregate in an asphalt mixture for rapid induction heating to hot mix temperatures. Herein, using 7.5% CS and 7.5% G replacement, a 5 gal tube of iHMA could be heated to approximately 320°F in 5 min or less. It is possible the required heating time could be reduced even further if, for example, CW was used in place of G. However, the focus of this project was feasibility, and, given the ability to meet heating objectives, this discussion summarizes general findings and focuses on other practical factors that may need to be considered.

## 7.1 Material properties

Relative to CMA, iHMA is expected to provide longer patch life since it essentially is HMA, which is the preferred material for patching. Most CMAs are solvent-based, emulsion-based, or contain epoxy additives, meaning they generally have a limited shelf life after which they are no longer useable. While long-term storage of iHMA has not yet been investigated, premature curing, as with CMA, would not be an issue.

Relative to HMA, iHMA appears to provide equivalent rutting resistance based on the data presented. The primary advantages of iHMA relative to HMA are its ability to be used in cold weather or in remote locations when conventional HMA is not available. If HMA were available in metal buckets, even then the time to heat an HMA bucket to 300°F is measured in hours, not minutes. Instead, iHMA can be heated quickly and on demand as needed.

Regarding the heating of iHMA, it has been suggested by several individuals that the mineral aggregate should provide some induction heating capacity. To investigate this, a small experiment was conducted where a blend of AC1 aggregates (i.e., no steel aggregates) was subjected to a 3.5 min heating cycle. $T_{int}$ increased from 71°F to only 78°F, which was most likely due to self-heating of the thermocouple considering how quickly temperature returned to 71°F after the heating cycle ended. Thus, it seems clear that it is not possible to inductively heat traditional HMA materials absent the steel aggregates.

Several challenges were encountered with iHMA such as the difficulty in $G_{sb}$ of FAA measurement or in cutting cores. These issues should perhaps be explored further in future studies. In the meantime, it is beneficial to recall that iHMA is intended for patching and not paving, which leads to greater allowable tolerances for some of the conventionally more critical properties like $G_{sb}$ and $V_a$. For example, $V_a$ level is never checked for patching, so the inability to core iHMA when used for a patch is less significant.

## 7.2 Repair times

Repair time is a practical operations consideration that has yet to be evaluated in depth. HMA repairs in this project were slightly faster than iHMA repairs, but the HMA was already heated. Downtime that the patching team may have experienced while waiting on iHMA tubes to be heated was not explicitly recorded in this project. From a qualitative perspective, there was little downtime, and both teams remained adequately occupied with tasks. For repairs larger than those performed in this project, there would be some additional downtime as several iHMA tubes may need to be heated, set aside, and then all used at once. However, this downtime could be productive as well if the patching team were able to perform any necessary preparatory work (e.g., saw cutting, base repair, etc.)

## 7.3 Cost information

Because this was a feasibility study from a technical perspective, cost was not a first-order concern. At this point, production-scale cost is unknown; however, it is an important consideration with respect to full-scale operations. Similar to spray-injection patchers for conventional pothole patching or the Bagela recycler for typical RADR processes, there would be an initial equipment cost for the FIH, followed by recurring materials costs. FIH costs are anticipated to be less than that of spray-injection patchers, and preliminary estimates indicate iHMA would be more expensive than most CMAs but less than premium CMAs such as AQUAPATCH or Instant Asphalt.

Pricing estimates were obtained from a single vendor for the steel materials tested in this project. Nominally speaking, B and G were more economical at approximately $0.50 per lb, whereas CS and CW were approximately $1.00 per lb. Conventional mineral aggregates are orders of magnitude cheaper at $15 to $20 per ton, meaning aggregate cost would be well under $1 for an entire 5-gal iHMA tube. Although more expensive at

approximately $500 per ton, asphalt binder cost would still be only about $1 per iHMA tube. The components needed to assemble a fiber tube container cost approximately $7.50.

Altogether, the materials needed to produce one 5-gal iHMA tube (7.5CS-7.5G blend) would be about $25 to $30. This number could increase or decrease depending on the steel used. For example, the 7.5CS-7.5CW blend would be closer to $35 per 5-gal tube, whereas the 7.5G-7.5G blend would be closer to $20 per 5-gal tube. Although not discussed in Section 5.2, costs were also considered as another factor when the 7.5CS-7.5G blend was selected as it balanced economics with other factors considered. The 7.5CS-7.5CW blend, which exhibited better heating properties, would pose a tradeoff with economics, and vice versa for the 7.5G-7.5G blend.

Relative to other materials such as CMAs, it must be considered that iHMA costs presented are materials costs and do not necessarily represent retail costs of a final pre-packaged iHMA tube; however, it may provide some indication of approximate cost for discussion. Because of the added steel, iHMA would cost significantly more than conventional HMA, which is currently about $60 per ton or about $2.25 per 5-gal bucket. This seems significant until CMAs are considered. The current standard Instant Road Repair CMA is currently about $16 per 3.5-gal bucket ($23 per 5-gal bucket), and the most recently recommended CMA (e.g. AQUAPHALT, Instant Asphalt) ranges from $50 to $100 per 3.5-gal bucket ($71 to $141 per 5-gal bucket). Overall, iHMA costs appear manageable when considering CMA costs and the improved performance achieved.

## 7.4 Envisioned usage

As it has been implied throughout the report, the envisioned use of iHMA would be to produce a bulk volume of iHMA mix as in normal hot mix plant production. This mix would then be packaged into 5-gal containers in a similar manner to pre-packaged CMA. iHMA tubes could then be distributed and staged as needed for operations. For example, iHMA could replace Instant Road Repair in the SuPR kit or be used to supplement RADR operations for small repairs where the entire asphalt RADR process is unnecessary.

# 8 Conclusions and Recommendations

The objective of this project was to perform a feasibility investigation of induction heating technology as a mechanism to heat small quantities of HMA in a matter of several minutes. The goal was to heat a 5 gal container of inductive HMA (iHMA) in approximately 5 min to 300°F (objective) or, at a minimum, 250°F (threshold). This objective was met using 15% steel aggregate in the aggregate blend, producing a mix that withstood simulated F-15E traffic.

## 8.1 Conclusions

Key conclusions resulting from this work are as follows:

1. The use of multiple steel materials of various particles sizes and shapes demonstrated the ability to produce an inductive hot mix asphalt material when dispersed as inductive aggregates in an asphalt mix.
2. iHMA heating test results were a function of steel content, type, and size, as well as container size, induction heater settings, and heating duration. In particular, this indicated iHMA mixes could be designed to achieve different heating characteristics to meet various needs. For example, various mixes can be designed that heat faster, retain heat longer, etc.
3. For this feasibility study, an iHMA blend containing 7.5% cube shot (CS) and 7.5% grit (G) by volume (15% total volume replacement of original mineral aggregate) was selected as a blend that balanced multiple properties (e.g., heating rate, peak temperature, heat retention, aggregate angularity, and cost).
4. Volumetric mix designs can be performed for iHMA just as for HMA with the primary difference being a larger dependence on volume-based properties (e.g., $V_{be}$) than mass-based properties (e.g., $P_b$). Conventional rules of thumb with mass-based properties were less informative for iHMA due to the large difference in specific gravity of steel and mineral aggregates.
5. There are several challenges introduced into normal testing and mix design when using steel aggregates. Of note in this project were fine aggregate angularity (FAA) and bulk specific gravity ($G_{sb}$) measurement and cutting of cores from in-place patches. Fortunately, these types of properties and activities that are common for conventional HMA are less critical for patch repair materials.

6. Using a prototype field induction heater, 5 gal containers of iHMA mix were successfully heated, achieving temperatures of 320°F in 5 min or less.
7. Full-scale testing of iHMA demonstrated its ability to be used for patch repairs similarly to CMA or HMA. Rutting results for iHMA under simulated F-15E traffic were comparable to and slightly less than that of HMA. Both exhibited considerably less rutting than the proprietary CMA (Instant Asphalt).
8. Induction heating appears to be a feasible technology for heating small quantities, such as a 5 gal container, of iHMA. As a feasibility study, this project demonstrated lab-scale to full-scale feasibility in order to provide a practice-ready concept.

## 8.2 Recommendations

The overall recommendation from this project is to re-evaluate each area of the iHMA concept (e.g., container selection, laboratory mix design, field placement, etc.) as each area has room for refinement. Specific recommendations from this work are as follows:

1. This work utilized fiber drum containers (e.g., mailing tubes, Sonotubes®) for iHMA. Long-term durability would be the primary concern of fiber containers; therefore, more robust but also economical container options should be explored.
2. Additional iHMA mixes should be designed using other steel aggregates beside the 7.5% CS and 7.5% G blend. These additional mixes should target specific design properties (e.g., longer heat retention for larger repairs).
3. More advanced laboratory characterization needs to be explored in order to fully quantify performance aspects of iHMA relative to conventional HMA and CMA materials
4. Given the F-15E load cart issues encountered in this project, additional field testing should be performed. This full-scale patching repair work should be expanded relative to this project to include a broader collection of iHMA mixes and possibly HMA and CMA mixes as well.
5. Weathering of iHMA over time, primarily the extent and effects of steel aggregate rusting, should be evaluated to ensure iHMA will not present foreign object debris (FOD) concerns.
6. Repair times and procedures need to be refined and finalized and documented in TTP format for potential incorporation at a later date.

# References

Ahmedzade, P. and B. Sengoz. 2009. Evaluation of steel slag as coarse aggregate in hot mix asphalt concrete. *Journal of Hazardous Materials* 165:300-305.

American Association of State Highway and Transportation Officials (AASHTO). 2010. *Standard method of test for determining the rutting susceptibility of hot mix asphalt (HMA) using the asphalt pavement analyzer (APA)*. Designation T340-10. Washington, DC: American Association of State Highway and Transportation Officials.

American Society for Testing and Materials (ASTM). 2011. *Standard test method for theoretical maximum specific gravity and density of bituminous paving mixtures*. Designation D2041-11. West Conshohocken, PA: American Society for Testing and Materials.

_____. 2015. *Standard test method for relative density (specific gravity) and absorption of coarse aggregate*. Designation C127-15. West Conshohocken, PA: American Society for Testing and Materials.

_____. 2015. *Standard test method for relative density (specific gravity) and absorption of fine aggregate*. Designation C128-15. West Conshohocken, PA: American Society for Testing and Materials.

_____. 2017. *Standard test methods for uncompacted void content of fine aggregate (as influenced by particle shape, surface texture, and grading)*. Designation C1252-17. West Conshohocken, PA: American Society for Testing and Materials.

_____. 2018. *Standard test method for bulk specific gravity and density of compacted asphalt mixtures using automatic vacuum sealing method*. Designation D6752-18. West Conshohocken, PA: American Society for Testing and Materials.

Cox, B. C., J. F. Rushing, and W. Floyd. 2017. *Rutting performance of cold-applied asphalt repair materials for airfield pavements*. ERDC/GSL TR-17-10. Vicksburg, MS: U.S. Army Engineer Research and Development Center.

Cox, B. C., and J. B. Sprouse. 2019. Characterization of Hot Mix Asphalt Patching Materials Produced with Medium-Scale Field Mixing Equipment. In *Proceedings of the 7th International Conference on Bituminous Mixtures and Pavements, 12-14 June*. Thessaloniki, Greece: Hyatt Regency.

Dailey, J., E. V. Dave, M. Barman, and R. D. Kostick. 2017. *Comprehensive field evaluation of asphalt patching methods and development of simple decision trees and a best practices manual*. Report MN/RC 2017-25. St. Paul, MN: Minnesota Department of Transportation.

Dong, Q., B. Huang, and S. Zhao. 2014. Field and laboratory evaluation of winter season pavement pothole patching materials. *International Journal of Pavement Engineering* 15(4):279-289.

Garcia, A., E. Schlangen, M. van de Ven, and Q. Liu. 2009. Electrical conductivity of asphalt mortar containing conductive fibers and fillers. *Construction and Building Materials* 23:3175-3181.

Garcia, A., E. Schlangen, M. van de Ven, and D. van Vliet. 2011. Crack repair of asphalt concrete with induction energy. *HERON* 56(1):33-44.

Garcia, A., M. Bueno. J. Norambuena-Contreras, and M.N. Partl. 2013. Induction healing of dense asphalt concrete. *Construction and Building Materials* 49:1-7.

Ghosh, D., M. Turos, M. Hartman, R. Milavitz, J. L. Le, and M. Marasteanu. 2018. *Pothole prevention and innovative repair*. Report 2018-14. St. Paul, MN: Minnesota Department of Transportation.

Latta, J. 2013. *A magic mix of magnetite and microwaves offers a super year-round pothole fix*. Equipment World's Better Roads. https://www.equipmentworld.com/hot-holes.

Liu, Q., E. Schlangen, M. van de Ven, and A. Garcia. 2010. Healing of porous asphalt concrete via induction heating. *Road Materials and Pavement Design* 11 (sup1):527-542.

Liu, Q., A. Garcia, E. Schlangen, and M. van de Ven. 2011. Induction healing of asphalt mastic and porous asphalt concrete. *Construction and Building Materials* 25:1746-3752.

Liu, Q., E. Schlangen, and M. van de Ven. 2012a. Induction healing of porous asphalt. *Transportation Research Record: Journal of the Transportation Research Board* 2305:95-101.

Liu, Q., E. Schlangen, M. van de Ven, G. van Bochove, and J. van Montfort. 2012b. Evaluation of the induction healing effect of porous asphalt concrete through four point bending fatigue test. *Construction and Building Materials* 29:403-409.

Liu, Q., E. Schlangen, and M. van de Ven. 2013a. Characterization of the material from the induction healing porous asphalt concrete trial section. *Materials and Structures* 46:831-839.

Liu, Q., E. Schlangen, and M. van de Ven. 2013b. Induction healing of porous asphalt concrete beams on an elastic foundation. *Journal of Materials in Civil Engineering* 25(7):880-885.

McDaniel, R. S., J. Olek, A. Behnood, B. Magee, and R. Pollock. 2014. *Pavement patching practices*. NCHRP Synthesis 463. Washington, DC: Transportation Research Board.

Mejías-Santiago, M., F. Valle-Roldán, and L. P. Priddy. 2010. *Certification tests on cold patch asphalt repair materials for use in airfield pavements*. ERDC/GSL TR-10-14. Vicksburg, MS: U.S. Army Engineering Research and Development Center.

Prowell, B., and A. Franklin. 1995. *Evaluation of cold mixes for winter pothole repair*. Publication VTRC 96-R9. Richmond, VA: Virginia Transportation Research Council, Virginia Department of Transportation.

Rudolph, R., P. Mitschang, and M. Neitzel. 2000. Induction heating of continuous carbon-fibre-reinforced thermoplastics. *Composites: Part A* 31:1191-1202.

Saeed, A., R. C. Mellerski, and M. I. Hammons. 2009. *Pelletized asphalt for airfield damage repair*. Report AFRL-RX-TY-TR-2010-0030. Tyndall Air Force Base, FL: Air Force Research Laboratory.

USAF, Air Force Civil Engineer Center. 2018. *Interim tactics, techniques, and procedures (TTPs); interim process for rapid airfield damage repair (RADR).* Rev 11.2. Washington, DC: Department of Defense.

Wilson, T. P., and A. R. Romine. 1999. *Materials and procedures for repair of potholes in asphalt-surfaced pavements – manual of practice*. Report FHWA-RD-99-168. McLean, VA: Federal Highway Administration.

Wu, S., L. Mo, Z. Shui, and Z. Chen. 2005. Investigation of the conductivity of asphalt concrete containing conductive fillers. *Carbon* 43:1358-1363.

Zanko, L. M., D. M. Hopstock, and W. DeRocher. 2016. *Evaluate and develop innovative pavement repair and patching: taconite-based repair options.* Report MN/RC 2016-03. St. Paul, MN: Minnesota Department of Transportation.

# Unit Conversion Factors

| Multiply | By | To Obtain |
|---|---|---|
| degrees Fahrenheit | (F-32)/1.8 | degrees Celsius |
| feet | 0.3048 | meters |
| gallons (U.S. liquid) | 0.1336 | cubic feet |
| inches | 0.0254 | meters |
| miles per hour | 0.44704 | meters per second |
| pounds (mass) | 0.45359237 | kilograms |
| square feet | 0.09290304 | square meters |
| square yards | 0.8361274 | square meters |
| yards | 0.9144 | meters |

# REPORT DOCUMENTATION PAGE

*Form Approved*
*OMB No. 0704-0188*



| 1. REPORT DATE *(DD-MM-YYYY)* | 2. REPORT TYPE | 3. DATES COVERED *(From - To)* |
|---|---|---|
| April 2020 | Final | |

**4. TITLE AND SUBTITLE**

Feasibility Investigation of Inductive Heating of Asphalt Repair Materials

**5a. CONTRACT NUMBER**

**5b. GRANT NUMBER**

**5c. PROGRAM ELEMENT NUMBER**

**6. AUTHOR(S)**

Ben C. Cox, Web C. Floyd, John F. Rushing, Thomas A. Carr, and Craig A. Rutland

**5d. PROJECT NUMBER**
463347

**5e. TASK NUMBER**

**5f. WORK UNIT NUMBER**

**7. PERFORMING ORGANIZATION NAME(S) AND ADDRESS(ES)**

Geotechnical and Structures Laboratory
U.S. Army Engineer Research and Development Center
3909 Halls Ferry Road
Vicksburg, MS 39180-6199

**8. PERFORMING ORGANIZATION REPORT NUMBER**

ERDC/GSL TR-20-10

**9. SPONSORING / MONITORING AGENCY NAME(S) AND ADDRESS(ES)**

Headquarters, Air Force Civil Engineer Center
139 Barnes Ave., Suite 1
Tyndall AFB, FL 32403-5319

**10. SPONSOR/MONITOR'S ACRONYM(S)**

AFCEC

**11. SPONSOR/MONITOR'S REPORT NUMBER(S)**

**12. DISTRIBUTION / AVAILABILITY STATEMENT**

Approved for public release; distribution is unlimited.

**13. SUPPLEMENTARY NOTES**

Rapid Airfield Damage Recovery (RADR) Program; MIPR Numbers F4ATA76307GW01 and F4ATA76307GW01 AMD 1

**14. ABSTRACT**

Airfield pavement repairs conducted as part of rapid airfield damage recovery (RADR) activities must utilize suitable materials to reduce the need for subsequent repairs in order to maintain an operable pavement surface. For asphalt concrete pavements, hot mix asphalt (HMA) is typically used, but this requires a fairly large operation and is less practical for small repairs (e.g., small munitions damage, potholes). Instead, cold mix asphalt (CMA) is typically used for small repairs; however, its performance under aircraft loads is generally unacceptable.

The objective of this project was to investigate the feasibility of rapidly heating small-repair quantities (e.g., 5 gal buckets) of asphalt mix to hot mix temperatures in a matter of minutes. This objective was met using 15% steel aggregate by volume to produce an inductive HMA (iHMA) that could be heated from ambient to 320°F in approximately 5 min. This technology was demonstrated at full scale with a prototype field induction heater; iHMA patch repairs were subjected to simulated F-15E traffic and exhibited comparable rutting resistance to conventional HMA, which was considerably improved relative to CMA. Overall, iHMA was found to be a feasible repair material and should be considered for additional refinement and eventual implementation.

**15. SUBJECT TERMS**

Asphalt
Induction heating
Pavement repair materials
Rapid airfield damage repair
Runways (Aeronautics)—Maintenance and Repair
Military bases
Pavements, Asphalt
Pavements, Asphalt--Testing

| 16. SECURITY CLASSIFICATION OF: | | | 17. LIMITATION OF ABSTRACT | 18. NUMBER OF PAGES | 19a. NAME OF RESPONSIBLE PERSON |
|---|---|---|---|---|---|
| a. REPORT | b. ABSTRACT | c. THIS PAGE | | | 19b. TELEPHONE NUMBER *(include area code)* |
| Unclassified | Unclassified | Unclassified | SAR | 66 | |